Materials Horizons

ROYAL SOCIETY OF CHEMISTRY

REVIEW

View Article Online
View Journal | View Issue

Cite this: *Mater. Horiz.*, 2026, 13, 2767

Photoplasticity behavior in inorganic semiconductors: unraveling fundamental mechanisms across ionic and covalent systems

Chengchi Cao and Qi An *

Inorganic semiconductors exhibit photoplasticity, where light exposure alters dislocation-mediated plastic flow based on the material's bonding character and carrier–defect interactions. In ionic II–VI compounds (*e.g.* ZnS and ZnO), above-band-gap illumination generates electron–hole pairs that are readily trapped at dislocation cores. This increases the Peierls stress (the effective barrier to glide), causing photoplastic hardening or a positive photoplastic effect. In contrast, covalent semiconductors (*e.g.* GaP, GaAs, Ge, and Si) demonstrate softening under illumination (negative photoplasticity) since photoexcited carriers often facilitate dislocation glide and reduce flow stress. This review summarizes recent experimental and theoretical progress on photoplasticity in inorganic semiconductors and integrates these results into a unified microscopic framework. Here, we discuss how modern techniques, density functional theory (DFT), constrained DFT, machine learning interatomic potentials, and large-scale molecular dynamics (MD) directly connect electronic excitation to changes in generalized stacking-fault energy surfaces, dislocation core reconstruction, and mobilities. On the experimental side, we review *in situ* mechanical tests under controlled illumination—from bulk compression to photo-nanoindentation and transmission electron microscopy—that directly show how light modulates dislocation activity. By systematically comparing ionic II–VI and covalent III–V/group-IV systems, we identify the key mechanisms that control the sign and magnitude of photoplasticity and outline design principles for semiconductors whose mechanical properties can be actively tuned by light illumination.

Received 5th December 2025,
Accepted 12th January 2026

DOI: 10.1039/d5mh02333e

rsc.li/materials-horizons

Wider impact

Light-induced plasticity offers a new approach for controlling the strength and ductility of optoelectronic and structural semiconductors. Recent advances reveal that moving dislocations can carry substantial nonequilibrium charge, and adjusting this charge with illumination can either impede or enhance dislocation motion. DFT, constrained DFT and machine-learned interatomic potentials now make it possible to model these carrier–dislocation interactions quantitatively at the atomic scale, linking electronic excitation to changes in Peierls stresses and dominant deformation modes. For practical applications, light-activated hardening could improve the reliability of devices under intense illumination—such as LEDs, laser diodes, and power electronics—by suppressing dislocation-mediated degradation. Conversely, light-induced softening suggests new routes for illumination-assisted forming, defect annealing, or shape programming in crystals. By mapping how bonding character, defect chemistry, and carrier dynamics jointly determine photoplastic response, this review aims to guide the rational design of materials whose mechanical behavior can be switched or continuously tuned using light.

1. Introduction

Photomechanical effects–changes in a material's mechanical behavior induced by light–have been observed in a variety of inorganic semiconductors for decades.[1–6] In particular, photoplasticity refers to the alteration of plastic deformation and dislocation-mediated flow under illumination. Depending on the material's bonding character, light can either strengthen or soften a semiconductor's plastic response. For example, ZnS, ZnO, ZnTe, CdTe and CdS crystals exhibit much more ductility in complete darkness than under UV light: illumination causes a positive photoplastic effect, *i.e.* light hardens the material while decreasing the ductility.[1,2,5,7–19] In contrast, covalent semiconductors, such as those based on Ge, Si, and GaX (X = P, As, and N), often show negative photoplasticity, where light softens the material.[2,4,20–22] In other words, exposure to above-band-gap light can increase flow stress in several ionic semiconductors but decrease it in covalent semiconductors.

Department of Materials Science and Engineering, Iowa State University, Ames, IA 50011, USA. E-mail: qan@iastate.edu

Understanding photoplasticity is crucial for the functioning of photovoltaic devices that operate under intense illumination (*e.g.* LED chips and laser-irradiated components) and opens possibilities for on-demand mechanical control, such as tuning strength or ductility, using light during processing.[23–35] Early electro- and photo-plasticity studies (Petrenko and Whitworth,[36] Osip'yan,[7] and others[37–41]) have established that moving dislocations in II–VI semiconductors carry an electric charge, act as electrically active objects, and directly couple their electrical properties to plastic flow. In a series of II–VI compounds (*e.g.* ZnO, ZnS, ZnSe, ZnTe, CdS, CdSe, and CdTe), electrical current during plastic deformation was measured, showing that this current is predominantly carried by the moving dislocations themselves and not by the bulk-free carriers. As a charged dislocation glides through the crystal, it transports net charge and generates a measurable electrical current, commonly termed a ''dislocation current'', that correlates with the crystal's flow stress.

These experiments[20,42–44] (on oriented single crystals under compression, with slip systems known or inferred) revealed several key trends. First, moving dislocations carry considerable nonequilibrium charges (electrons or holes captured or emitted from defect states), often a significant fraction of an electron per Burgers vector length. The sign of this charge follows the doping character of the host: n-type ZnS, ZnSe, CdS, CdSe, and CdTe have negatively charged moving dislocations, whereas p-type ZnTe has positively charged dislocations. Second, illumination was shown to increase the magnitude of the dislocation charge and the flow stress (positive photoplastic hardening) in most of these II–VI crystals. This hardening is not broadband; its spectral maximum appears at $\sim 0.9\ E_g$, which means that the effect is strongest when the photon energy is just below the threshold for band-to-band absorption. For example, in ZnS, light can boost the charge of mobile partial dislocations to nearly the full ionic limit and simultaneously increase the stress required for continued slip. Essentially, these tests (including magnetic-field ''Hall'' measurements[45,46]) showed that the increased current cannot be explained by ordinary photocarriers: the current tracks the dislocations' motion and charging state, with bulk carriers contributing at most a few percent.

Petrenko and Whitworth[36] interpreted this tight charge–stress correlation using a dynamic-charge model. A gliding dislocation in these partly ionic II–VI crystals inherently carries an ''ionic'' core charge (due to crystal asymmetry); however, it continuously exchanges carriers with nearby traps and the bands as it moves. The dislocation core hosts mid-gap electronic levels (donor- or acceptor-like) from reconstructed and dangling bonds. As the dislocation sweeps through the lattice, it ''scoops up'' carriers from local traps and loses others by tunneling to the bands. In a steady state, the moving dislocation acquires a large nonequilibrium line charge, set by a balance of capture and emission rather than thermal equilibrium. This charge can greatly exceed what the bulk would screen, even reversing sign relative to the naïve ionic picture depending on doping. Importantly, a highly charged core must drag this charge distribution through the periodic lattice potential, increasing the effective resistance to motion (the Peierls barrier) and hence the flow stress. Under illumination tuned near $0.9 \times E_g$, the core states are more effectively populated (or depopulated); thus, the moving dislocation gains an even greater nonequilibrium charge, and the flow stress increases accordingly. In short, intense light increases dislocation charge, which increases lattice resistance and therefore raises the flow stress (positive photoplastic hardening). In contrast, in covalent semiconductors such as Ge or GaP, other studies observed an opposite trend (light-assisted softening). Thus, the robust ''light hardens'' behavior in II–VI materials provides a baseline: photoplasticity is an electromechanical effect at the dislocation core, not a trivial heating effect. It establishes the direct quantitative association between (i) nonequilibrium line charge on a dislocation and (ii) the stress required to move it, which becomes the foundation for comparing ''light hardens'' systems (ZnS, ZnSe, *etc.*) against ''light softens'' systems (GaP, GaAs, *etc.*) in a unified photoplasticity framework. Osip'yan *et al.*[39] further confirmed this picture: in II–VI semiconductors, moving dislocations carry a large nonequilibrium charge (scooped from defect states), producing a measurable current, and light application increases the charge and flow stress. Again, the spectral maximum lies just below the band gap.

These reviews[36,39] have consolidated this body of work: they detailed how the dislocation-current technique is employed to extract the line charge under controlled compression and when the photoplastic effect can change sign. For example, a prismatic slip in wurtzite CdS/CdSe can show small hardening at a low light intensity that switches to softening at a higher intensity (negative photoplasticity) with a narrower spectral response. Polycrystalline or work-hardened CdTe can also shift from positive to negative photoplasticity with increasing illumination. Temperature trends have been quantified: hardening weakens at higher temperatures, and wider-gap materials

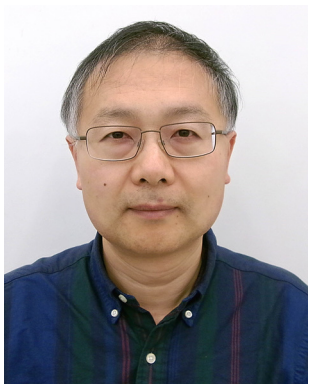

Qi An

Qi An is an Associate Professor in the Department of Materials Science and Engineering at the Iowa State University. He received his MS and PhD degrees in Materials Science from Caltech and his BS degree from the University of Science and Technology of China. His research area is computational materials science covering machine learning, electronic structure calculations, and atomistic simulations. His research specifically focuses on the mechanical properties of superhard ceramics, semiconductors, and thermoelectric materials; computational alloy design; batteries; metallic glasses; material behaviors under extreme conditions; and heterogeneous catalysis.

retain the effect to higher T. Long-lived after-effects (photoplastic responses persisting up to 10^4 seconds after the light is turned off) are observed, which are attributed to traps near the core or long-lived core states. Competing mechanisms are discussed (*e.g.* point defect-limited glide at a higher T), and a competition model is proposed where linear *vs.* quadratic charge-dependent terms in the kink-formation energy can reverse the sign of the effect. This elucidates the conditions where the charge-control model dominates and where other processes may prevail.

Overall, various mechanisms have been proposed to explain photoplasticity, all involving interactions between photoexcited carriers and crystal defects. Dislocations can carry charged states and alter local bonding; the injection of electron–hole (e–h) pairs may change the dislocation core structure, raise or lower the Peierls stress (the critical stress to move a dislocation), or even activate different deformation modes. Carriers trapped at dislocation cores can ''pin'' them (hardening), whereas carriers can also screen long-range forces or provide energy to break bonds (softening). Early studies on GaAs, Si, and Ge under electron-beam irradiation (analogous to injecting carriers) reported enhanced dislocation mobility, attributed to recombination-enhanced dislocation glide (non-radiative recombination at the core lowers the activation energy for motion).[20,47–49] However, a comprehensive microscopic understanding of photoplasticity remains elusive. Recent advances in experimental techniques and atomistic simulations have begun to unravel these mechanisms in detail.

This review focuses on inorganic semiconductors, highlighting the differences between predominantly ionic *vs.* covalent bonding, their mechanistic origins, and emerging methods to study and harness these effects. Particularly, we discuss recent theory and experimental progress to develop a unified picture of photoplasticity. Below, we first discuss photoplastic phenomena in ionic II–VI compounds, then in covalent III–V and elemental semiconductors, followed by a direct mechanistic comparison. Furthermore, we review methodological advances (DFT, constrained DFT, machine learning interatomic potentials (or machine learning force field), *in situ* mechanical testing and characterization) providing these insights, propose material design principles, and outline future research directions.

2. Photoplasticity in II–VI ionic semiconductors

In strongly ionic II–VI semiconductors (ZnS, ZnO, ZnSe, CdTe, *etc.*), illumination generally suppresses plastic flow, giving rise to positive photoplasticity.[7,18,50–53] In ZnS, for example, *in situ* experiments revealed a clear transition in the deformation mode: an ordinary dislocation glide dominates in darkness, whereas under near-band-gap illumination, deformation proceeds primarily by twinning. Transmission electron microscopy further confirms a strong reduction in mobile dislocation density under illumination, suggesting that plastic strain becomes localized into twins rather than distributed by glide.[9]

2.1. Key features of ionic semiconductors relevant to photoplasticity

Ionic II–VI semiconductors, such as ZnS, ZnO and CdTe, are ideal materials systems to reveal light–mechanics coupling as their wide band gaps, mixed ionic–covalent bonding and abundant native point defects produce strongly charged dislocation cores whose mobility is exquisitely sensitive to carrier concentrations.[54–56] (i) Wide band gaps and deep defect states. ZnS and ZnO have wide gaps[57–60] and abundant deep defect states (*e.g.* vacancies and interstitials).[61–68] Illumination near the band edge can efficiently populate or empty these states at dislocation cores and nearby defects (such as oxygen vacancies in ZnO),[69] shifting core charge and altering lattice resistance. Experiments and theory consistently reveal suppressed dislocation glide under illumination in ZnS and orientation-dependent hardening in ZnO.[9,70,71] (ii) Ionicity and polarity. Mixed ionic–covalent bonds (and in wurtzite structures, polar axes) produce large dislocation core charges and anisotropic slip.[72–76] Light can stabilize alternate deformation modes (twinning or dislocation) or modify basal/pyramidal slip activity, resulting in strong anisotropy in the photoplastic response. (iii) Defect-chemistry tunability. As carrier trapping at native or intentional defects mediates the effect, growth and processing that control defect populations can dramatically alter photoplastic responses.[61,62,77–81] For example, defect engineering can tune photoelastic and photoplastic responses over wide ranges in ZnO, ZnS, and CdS.[54]

These ingredients unify decades of phenomenology with modern observations and directly associate plastic flow with carrier-controlled dislocation mobility. ZnO demonstrates large, orientation-dependent changes in hardness and creep when illumination is switched on or off, consistent with carrier-mediated modifications of dislocation activity. Recent first-principles calculations further resolve how illumination-induced charge-state changes reconstruct dislocation cores and elevate Peierls barriers in ZnS, thereby providing a mechanistic bridge from atomic-scale charging to macroscopic hardening.[9,82,83] In ionic II–VI semiconductors, photoplasticity follows a charge-controlled dislocation picture: light → carriers → defect/dislocation charging → core reconstruction and barrier modulation → changes in plasticity (flow stress, hardness, creep). This will serve as the baseline for comparison with more covalent semiconductors (GaP, GaAs, Si, and Ge), where reduced ionicity and different defect landscapes can invert the sign or magnitude of the photoplastic effect.

2.2. ZnS as a prototype: experimental evidence

Among II–VI compounds, cubic ZnS (sphalerite) provides the clearest experimental demonstration of light-inverted plasticity. Oshima *et al.*[9] conducted deformation tests on bulk ZnS single crystals under controlled illumination (room-temperature compression under white LED, 365-nm UV, and complete darkness) and correlated the mechanical response with microstructure (optical/temporal microscopy, TEM) and optical absorption.[9]

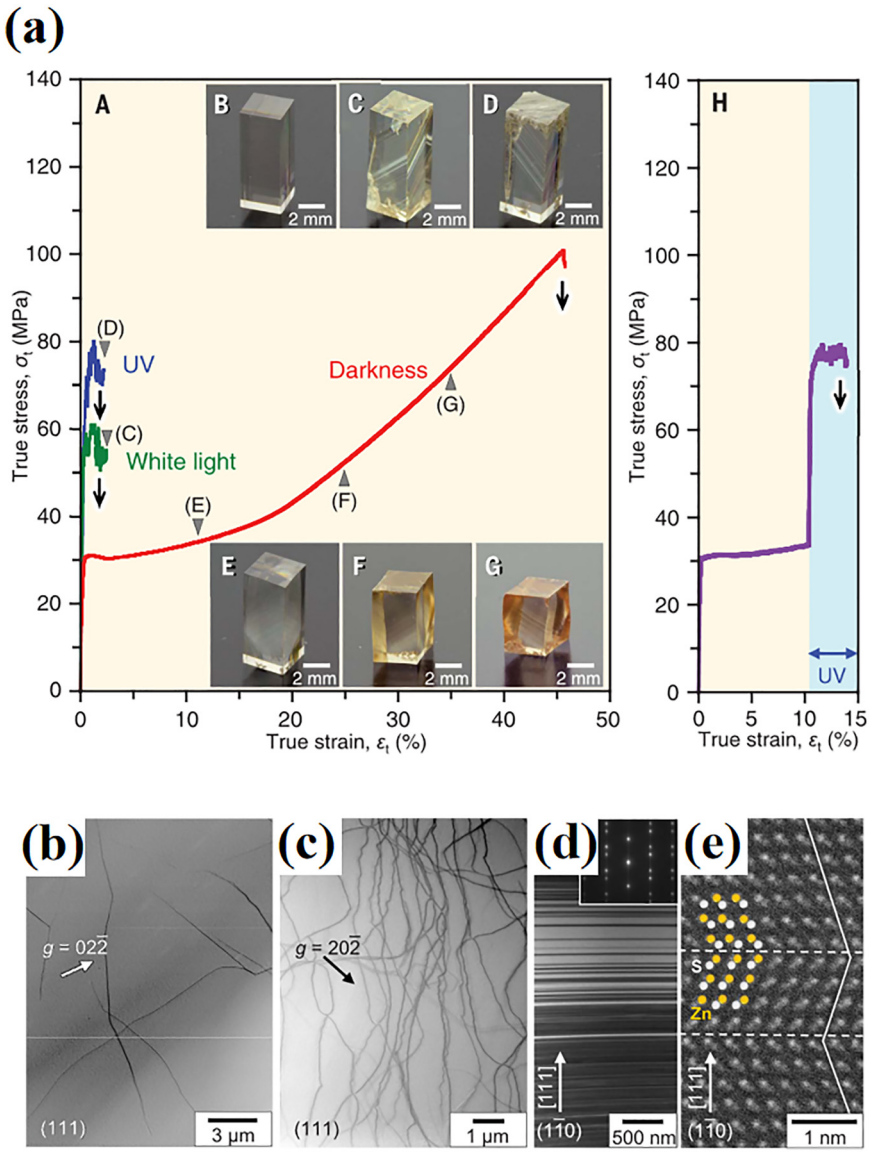

Fig. 1 (a) True stress–true strain response of single-crystal ZnS under different light conditions. Left: Curves acquired under a white LED, 365-nm UV, and complete darkness. Right: Deformation in darkness to ~10% strain followed by exposure to a 365-nm UV causes immediate brittle failure. (b) and (c) Bright-field STEM images of undeformed ZnS and a specimen deformed to 25% strain in darkness, showing a large increase in dislocation density. (d) Bright-field TEM image of a twinning region after UV deformation. (e) HAADF-STEM image of a crystal twin (scale bars: 3 μm, 1 μm, 500 nm, and 1 nm, respectively).[9] Copyright is from Science.[9]

Fig. 1(a) presents the true stress–strain response of single-crystal ZnS under various light conditions. Under white or UV light, the crystals essentially fracture at yield, exhibiting brittle failure. However, in complete darkness, ZnS sustains stable plastic flow up to ~45% true strain, with work hardening and a lower flow stress compared with illuminated cases. This stark difference anchors the central claim: darkness activates dislocation-mediated plasticity, while illumination restores brittleness. Strikingly, this control is reversible: a sample deformed in darkness to ~10% strain immediately fractured when UV light was turned on, directly demonstrating a light-induced brittle transition during ongoing deformation (Fig. 1(a) inset).

Under UV light, specimens exhibit prominent slip markings with deformation twins, whereas dark-deformed crystals show only faint, fine slip lines (homogeneous glide without twinning). Bulk STEM quantification (Fig. 1(b) and (c)) confirms that in darkness, the dislocation density jumps from $<10^7$ cm^{-2} (as-grown) to $\sim 5 \times 10^8$ cm^{-2} at 25% strain, with Burgers vectors of $\frac{1}{2}\langle 011\rangle$ on $\{111\}$ primary slip planes. This suggests that the multiplication and glide of dissociated partials serve as carriers of plasticity in darkness. Contrarily, illumination correlates with extensive twinning and far fewer glissile dislocations. These macroscopic and microscopic observations (Fig. 1) establish that ZnS is ductile when dark and brittle under illumination.

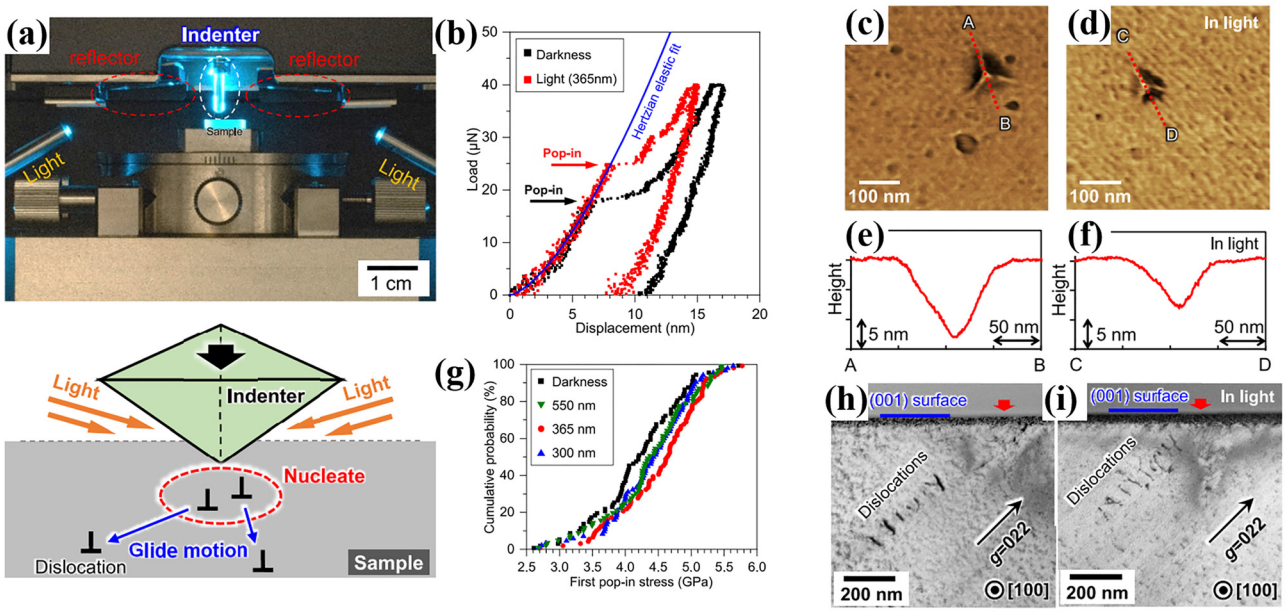

Fig. 2 Newly developed photo-nanoindentation platform. (a) Optical image of the setup under illumination. Two symmetrically arranged light paths and reflectors deliver controlled irradiation onto the sample during indentation. Schematic of light-assisted nanoindentation. The system irradiates the surface from low-angle directions (~16°) to avoid indenter-tip shadowing, ensuring uniform illumination of the contact region where dislocation nucleation and subsequent glide occur. The wavelength and intensity of the incident light are externally tunable in real time. (b) Representative load–displacement curves for nanoindentation on the ZnS (001) surface measured in darkness and under a 365-nm illumination. The blue line denotes the Hertzian elastic fit. Pop-in events, marked by abrupt displacement jumps deviating from the elastic response, are observed under both conditions. The overlap of the initial elastic portions indicates that the Young's modulus remains unchanged under illumination. (c and d) SPM phase images of the indented surfaces obtained in darkness (c) and under illumination (d). (e and f) Line profiles extracted along the A and B (dark) and C and D (light) traces highlighted in panels (c) and (d), respectively, showing comparable surface impressions but subtle differences in pile-up geometry. (h and i) Cross-sectional TEM images taken beneath the corresponding indents in darkness (h) and under illumination (i).[84] Figures are reproduced from ref. 84 under the terms of the Creative Commons CC BY 4.0 license.

To further elucidate this illumination-controlled plasticity at microscopic scales, Nakamura *et al.*[84] developed a precisely synchronized photo-nanoindentation platform (Fig. 2(a)) that can deliver controlled wavelengths (300–550 nm) and intensities across the entire surface, eliminating indenter-shadow artifacts. Load–displacement curves (Fig. 2(b)) show that under 365-nm near-band-edge illumination, the first pop-in stress increases by ~15% and the hardness by ~20%, while the indentation creep rates markedly drop—direct evidence that light increases the nucleation threshold and resistance to glide. Cross-sectional TEM beneath indents provides a crucial mechanistic insight. In darkness (Fig. 2(c), (e) and (h)), ZnS exhibits dense, deep-penetrating dislocation bundles extending far below the imprint, forming continuous slip bands characteristic of unhindered {111} ⟨110⟩ glide. However, under illumination (Fig. 2(d), (f) and (i)), dislocations become fewer, shorter, and confined near the surface, with markedly reduced glide distance. This directly confirms that photoexcitation suppresses propagation rather than nucleation, despite the modest (~15%) increase in nucleation stress. The wavelength-dependent statistics (Fig. 2(g)) demonstrate the strongest effect at 365 nm—consistent with maximal carrier generation near the 3.5–3.7-eV bandgap of ZnS. Both 300 nm (too strongly absorbed near the surface) and 550 nm (sub-bandgap, weak absorption) exert weaker effects, establishing penetration depth and carrier density as the key control parameters. Collectively, these observations demonstrate that photogenerated carriers elevate the effective Peierls barrier in ZnS, dramatically slowing down the dislocation glide while only slightly shifting nucleation. Thus, the correlation among scanning probe microscopy (SPM), pop-in statistics, and TEM microstructures provides the first nanoscale, real-space validation that illumination immobilizes dislocations in ZnS by hindering their motion.

Li *et al.*[8] further combined photo-nanoindentation, cross-sectional TEM, and atomistic simulations to directly visualize illumination-controlled dislocation dynamics in ZnS. They indented ZnS (depth ~600 nm) under darkness and controlled UV–IR illumination, thereby ensuring identical mechanical boundary conditions (Fig. 3(a)). The load–displacement curves (Fig. 3(b)) again exhibit clear light-induced hardening: under 365-nm light, the first pop-in occurs at a higher load, and the average hardness increases (~2.49 GPa in darkness → 2.99 GPa under illumination [Fig. 3(c)], consistent with earlier Vickers data). The hardness change ΔH peaks near 365 nm (Fig. 3(d)), confirming that photogenerated carriers, not heating, govern the effect. TEM and diffraction analyses revealed that in darkness, the indented region (Fig. 3(e) and (f)) contains dense, deep arrays of {111} slip dislocations with substantial lattice rotation (indicating large plastic strain). Under illumination, by contrast, the dislocation bundles are sparser, shorter,

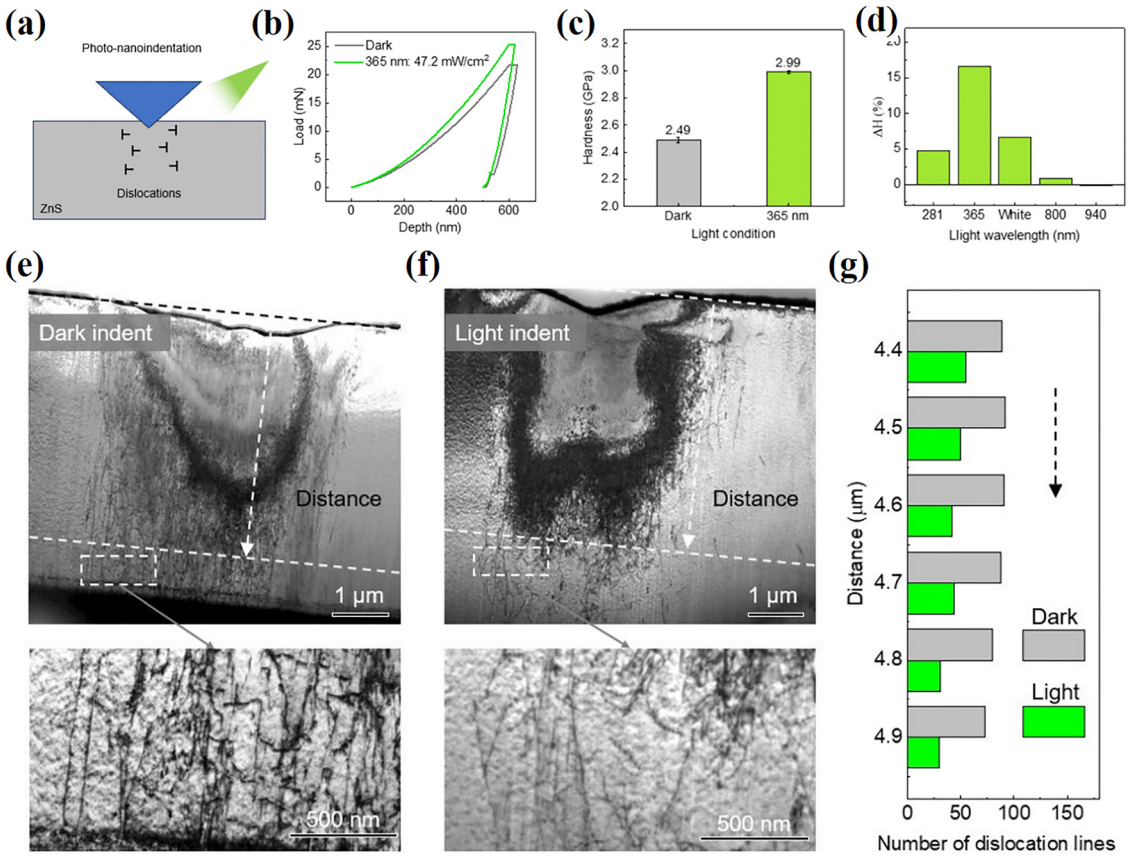

Fig. 3 Photo-nanoindentation response of ZnS measured in darkness and under illumination. (a) Schematic of the experimental configuration, illustrating light-assisted nanoindentation and the formation and propagation of dislocations beneath the indenter. (b) Representative load–depth curves collected in darkness (gray) and under a 365-nm illumination (green). Both indents were driven to a fixed depth of 600 nm, and light irradiation results in a higher pop-in load and enhanced resistance to plastic penetration. (c) Comparison of hardness values extracted from indentation experiments, showing an increase from 2.49 GPa in darkness to 2.99 GPa under the 365-nm illumination. (d) Wavelength-dependent change in hardness, ΔH, revealing a pronounced peak under near-band-edge excitation at 365 nm, while the sub-bandgap (800–940 nm) illumination produces negligible effects. (e) Cross-sectional TEM image of the dark indent, showing dense, deep-penetrating dislocation bundles that extend to several micrometers below the surface. The enlarged bottom-area (inset) highlights continuous dislocation lines characteristic of an unhindered {111} slip. (f) Corresponding TEM image under illumination. The dislocation bundles become shorter, sparser, and confined closer to the surface, with markedly reduced penetration depth relative to the dark condition. The enlarged view reveals a substantially diminished dislocation density. (g) Quantitative dislocation counts as a function of depth. At all sampled depths (4.4–4.9 μm), the number of dislocation lines is consistently lower in light indents, confirming that illumination suppresses dislocation propagation rather than nucleation.[8] Copyright is from Elsevier, Scripta Materialia.[8]

and confined near the surface (nearly 60% fewer dislocations at the indent bottom). Selected-area electron diffraction exhibits pronounced spot splitting and rotation under illumination—signatures of arrested dislocations and geometrically necessary dislocation boundaries. These observations directly confirm that light suppresses dislocation propagation (not nucleation), consistent with the creep reduction observed by Nakamura *et al.*[84]

At the atomic scale, Li *et al.* used DFT-trained machine learning interatomic potentials to study the 30° partial (the lowest-barrier carrier of plasticity in ZnS). DFT optimization shows that photoexcitation modifies the S-core structure of the 30° partial (notably altering Zn–S bond angles). Large-scale MD simulations of a dislocation dipole ($\sim 5.8 \times 10^5$ atoms) show that the Peierls stress for the 30° partial increases from ~1.38 GPa (dark) to ~1.64 GPa (excited). At fixed applied strain, the illuminated S-core glides a shorter distance than in darkness. Static calculations of the stress field show enhanced stress magnitudes around S- and Zn-core dislocations in the excited state, implying stronger dislocation–dislocation interactions. Collectively, these results quantitatively link photogenerated carriers to an elevated Peierls barrier and reduced glide mobility in ZnS.

In summary, the combined TEM quantification and atomistic modeling in Li *et al.*[8] provide a full mechanistic chain for ZnS: carrier trapping and redistribution at partial-dislocation cores elevate the glide barrier and reduce mobility, strengthening the material under illumination. This completes the story from Oshima's macroscopic brittle-ductile transition, through Nakamura's nanoscale validation, to Li *et al.*'s atomic-scale explanation.

2.3. Underlying mechanisms revealed by first-principles and atomistic simulations

With macroscopic and nano-mechanical studies now firmly establishing the phenomenology of positive photoplasticity in

ZnS, a clear trend has emerged: in darkness, ZnS exhibits extensive dislocation glide, whereas near–band-edge illumination hardens the crystal by shortening glide paths and markedly reducing dislocation density. However, these experiments cannot, on their own, reveal how photoexcited carriers modify the fundamental energy landscape governing the dislocation motion. Understanding this requires explicit treatment of the electronic structure, prompting the use of constrained-excitation first-principles calculations coupled with large-scale atomistic simulations.

A major advance came from Wang *et al.*,[85] who applied constrained DFT to quantify how band-gap excitation reshapes the generalized stacking-fault energy (GSFE) surface, $\gamma(u)$, in sphalerite ZnS and related II–VI compounds. By explicitly introducing electron–hole pairs and evaluating GSF energies along two {111} slip paths (Fig. 4(a)), they developed a twinnability metric that differentiates slip-dominated from twin-dominated deformation. In the ground state, ZnS exhibits a slip-favored landscape, consistent with its dark-state ductility. However, under photoexcitation, the difference between the unstable stacking-fault (γ_{us}) and twinning (γ_{ut}) energies narrows, causing a substantial increase in twinnability (Fig. 4(c)–(f)). This provides a direct microscopic explanation for the experimentally observed light-induced ductile-brittle transition, where ZnS shifts from dislocation-mediated plasticity in darkness to twinning-dominated failure under illumination.

Extending their analysis across the II–VI series, Wang *et al.* found that band-gap excitation systematically decreases γ_{us}, following the trend ZnS > ZnSe > ZnTe > CdTe. In ZnTe and CdTe, the γ_{us} values at the highest excitation level approach ~200 mJ m^{-2}—comparable to Mg or Al—indicating potentially metal-like ductility under strong illumination. Notably, twinnability in these narrower-gap materials remains unchanged or even decreases, favoring slip rather than twinning. Energy decomposition using a Madelung model shows that electron–hole pairs weaken long-range Coulomb interactions most strongly in wide-band-gap, highly ionic systems, such as ZnS, but less significantly in more covalent ZnTe and CdTe.

Collectively, these results establish a coherent electronic-structure picture: band-gap excitation modifies long-range ionic interactions and the GSF energy landscape (Fig. 4(b)), thereby dictating whether illumination promotes slip or twinning. This constrained DFT framework provides the first direct association between carrier redistribution and light-controlled deformation modes in II–VI semiconductors and lays the foundation for atomistic simulations that explicitly resolve dislocation cores, Peierls stresses, and carrier–defect interactions under illumination.

Although Wang *et al.* treated the effect of electronic excitation at the level of GSFE and twinnability, *i.e.* how homogeneous carrier excitation reshapes the slip–twin energy landscape in bulk ZnS and related II–VI compounds, their model does not explicitly resolve the atomic structure of dislocation cores themselves. To rationalize the ZnS photoplasticity, Matsunaga/Hoshino *et al.*[86] performed systematic DFT(+U) calculations on individual 30° and 90° glide partials with Zn-core (β) and S-core (α) characters. In the neutral state (q = 0), almost all cores relax back to unreconstructed configurations; only the 90°

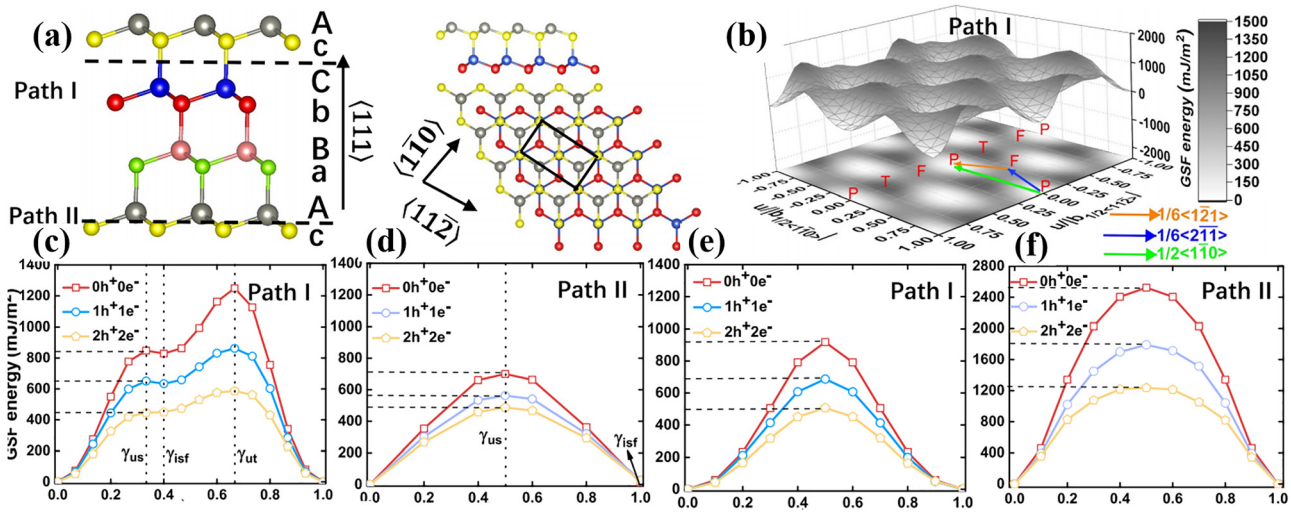

Fig. 4 (a) Schematic of the sphalerite ZnS stacking sequence AaBbCc along the ⟨111⟩ crystallographic direction, together with a top-down view of the {111} plane defined by the two in-plane normals ⟨11$\bar{2}$⟩ and ⟨1$\bar{1}$0⟩. Layers A, B, C and a, b, c correspond to Zn and S atomic planes, respectively. The black rectangles denote the Burgers vectors 1/2 ⟨11$\bar{2}$⟩ a_0 and 1/2 ⟨1$\bar{1}$0⟩ a_0. The dashed lines outline two possible slip trajectories on the {111} plane, referred to as paths I and II, which connect either widely spaced layers (*e.g.*, Cc) or closely spaced layers (*e.g.*, Ac). (b) Three-dimensional generalized stacking-fault (GSF) energy surface for path I obtained from DFT calculations, where P, F, and T denote the perfect lattice, unstable stacking fault, and unstable twinning fault, respectively. (c and d) GSF curves for path I (c) and path II (d), plotted as a function of the normalized displacement $u/|b|$ along ⟨11$\bar{2}$⟩, with b as the Burgers vector magnitude and u as the relative shear displacement. Results are shown for the ground state, the one electron–hole–pair excited state, and the two electron–hole–pair excited state (denoted as 0h$^+$0e$^-$, 1h$^+$1e$^-$, and 2h$^+$2e$^-$, respectively). The corresponding unstable stacking-fault, intrinsic stacking-fault, and unstable twinning-fault energies are labeled γ_{us}, γ_{isf}, and γ_{ut}, respectively. (e–f) GSF energy profiles for path I (e) and path II (f) along the ⟨1$\bar{1}$0⟩ direction.[85] Copyright is from the American Physical Society, Physical Review B.[85]

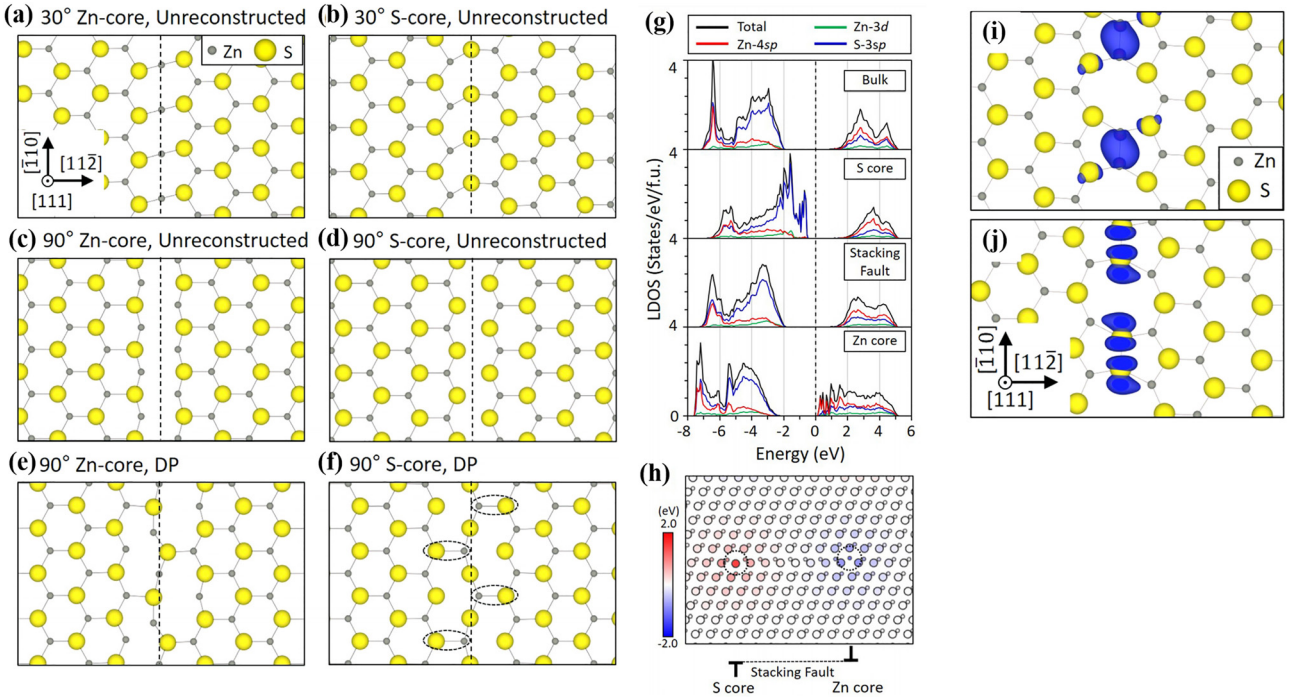

Fig. 5 Calculated atomic structures of Zn-core and S-core partial dislocations viewed normal to the (111) slip plane for the neutral state (q = 0). (a–c) 30° and 90° Zn-core configurations and (d–f) corresponding S-core structures. For each core type, both unreconstructed and double-period (DP) reconstructed geometries are presented. The dashed lines denote the dislocation lines. LDOS curves (g) and excess electrostatic potentials at atomic sites (h) around a pair of 30° partials before carrier trapping (q = 0). (i) and (j) Isosurfaces illustrating the localized electronic states that emerge around the dislocation core when carriers are captured.[86] Copyright is from Elsevier, Acta Materialia.[86]

Table 1 Core structures of partial dislocations in crystalline ZnS at the neutral state (q = 0) and their reconstruction energies, ΔE_{rc}, calculated as formation-energy differences relative to unreconstructed cores. Except for the 90° DP partials, all reconstructed cores relax back to their corresponding unreconstructed configurations[86,88]

Dislocation type	Initial model	After optimization	ΔE_{rc} (eV nm^{-1})
Zn core			
30°	DP	Unreconstructed	—
90°	SP	Unreconstructed	—
	DP	DP	−0.29 (ref. 86)
			−0.26 (ref. 88)
S core			
30°	DP	Unreconstructed	—
90°	SP	Unreconstructed	—
	DP	DP	+0.13 (ref. 86)
			+0.16 (ref. 88)

Table 2 Reconstruction energies, ΔE_{rc}, of Zn-core and S-core partial dislocations in ZnS for different charge states, q. Negative values indicate energetically favorable reconstructions[86]

Dislocation	Charge state (q)	ΔE_{rc} (eV nm^{-1})
Zn core		
30° DP	−2	−1.37 (ref. 86)
90° SP	−3	−0.24 (ref. 86)
90° DP	−3	−0.31 (ref. 86)
S core		
30° DP	+2	—
90° SP	+2	—
90° DP	+3	+0.13 (ref. 86)

DP cores are marginally more stable, with reconstruction energies $|\Delta E_{rc}| \lesssim 0.3$ eV nm^{-1} (Fig. 5(a)–(f)). Table 1 summarizes the DFT calculations on the core reconstruction energy from two recent studies.[86,88] The LDOS and electrostatic-potential maps (Fig. 5(g) and (h)) show that the S-core bands are shifted upward and the Zn-core bands downward relative to bulk, reflecting strong localized electrostatic fields of order ±2 eV that are confined to the core region.

Carrier trapping is treated by varying the dislocation charge state (q = −4… + 4) and computing formation energies as a function of Fermi level. For the 30° partials, the most stable states near the CBM/VBM correspond to q = −2 on Zn-core segments and q = +2 on S-core segments; in these charge states, the cores undergo double-period (DP) reconstruction with large energy gains: $\Delta E_{rc} \approx -1.37$ eV nm^{-1} for 30° Zn-core and ≈ -0.74 eV nm^{-1} for 30° S-core, whereas the 90° partials exhibit much smaller $|\Delta E_{rc}| \approx 0.2$–$0.3$ eV nm^{-1} (Table 2). Band-decomposed charge densities (Fig. 5(i) and (j)) show that the trapped electrons form deep Zn-4sp bonding states along the Zn-core rows, while the trapped holes empty S-3sp antibonding states at the S-cores, promoting robust DP reconstructions that were unstable or metastable in the pristine crystal.

These carrier-induced reconstructions markedly elevate the effective Peierls barrier for glide. Using the known correlation between ΔE_{rc} and kink-migration activation energies, the authors

estimate that replacement of the pristine 30° partial (Peierls barrier ≈ 0.4 eV nm^{-1}) by the charged reconstructed core ($|\Delta E_{rc}|$ ≳ 0.7–1.4 eV nm^{-1}) can reduce dislocation velocities at room temperature by ≲10^{-5}. As real dislocation loops in ZnS are built from 30°–30° and 30°–90° partial pairs, the highly pinned 30° segments dominate loop mobility, providing a microscopic explanation of why light-generated carriers harden ZnS and promote a ductile-brittle transition under illumination.

Building on the ZnS dislocation studies described above, Shen *et al.*[87] combined constrained DFT with *in situ* photo-nanoindentation to directly identify how photogenerated carriers—particularly holes —modify dislocation glide in II–VI semiconductors. On the computational side, they constructed a dipole consisting of 30° S-core and Zn-core partial dislocations in sphalerite ZnS and monitored the glide of each core while gradually introducing electron–hole pairs. Charge-density and density-of-states analyses revealed a pronounced asymmetry in carrier trapping, as illustrated in Fig. 6(a)–(d). The 30° S-core hosts a deep defect state just above the valence-band maximum; under illumination, holes strongly localize on this state and progressively straighten the bent Zn–S–Zn chain that characterizes the ground-state S-core. Contrarily, defect states are associated with the Zn-core hybridized with the conduction band; thus, photoelectrons remain broadly distributed and produce only minor structural changes. This asymmetry means that illumination primarily modifies S-core bonding, while the Zn-core remains comparatively inert—an essential distinction for understanding positive photoplasticity.

The consequences for dislocation mobility are quantified by computing the migration energy barrier of the 30° S-core as a function of e–h concentrations. The barrier demonstrates a characteristic non-monotonic dependence: it slightly decreases at a very low excitation, then sharply increases by roughly 40% at ∼0.5 e–h per 216-atom cell as the S-core defect state becomes filled with holes, and finally saturates once no additional carriers can be accommodated. These structural and energetic trends are illustrated in Fig. 6(a)–(e), which contrasts the carrier-free and hole-rich S-core configurations with the minimally perturbed Zn-core.

Essentially, *in situ* nanoindentation experiments on ZnS under 365-nm illumination show an almost direct experimental counterpart to the computed barrier trend. As light intensity increases, the hardness rises and then plateaus at a high flux, reflecting the calculated increase-and-saturation behavior of the S-core Peierls barrier (Fig. 6(f)). The close correspondence between simulation and experiment strongly suggests that hole trapping at the 30° S-cores is the dominant microscopic mechanism of positive photoplasticity in ZnS: illumination injects holes, strengthens S-core bonds, elevates the glide barrier, and thereby suppresses the dislocation motion.

Understanding how light alters the dislocation behavior requires simulations that simultaneously capture electronic excitation, core reconstruction, long-range stress fields, and collective dislocation motion. DFT excels at describing electronic structure but is limited to comparatively small cells and short timescales. Based on the aforementioned DFT-based insights, Luo *et al.*[88] extended the analysis by combining first-principles calculations with machine learning force fields (ML-FF) to quantify how photoexcitation alters the mobility of 30° and 90° partial dislocations with the Zn- and S-cores in ZnS.

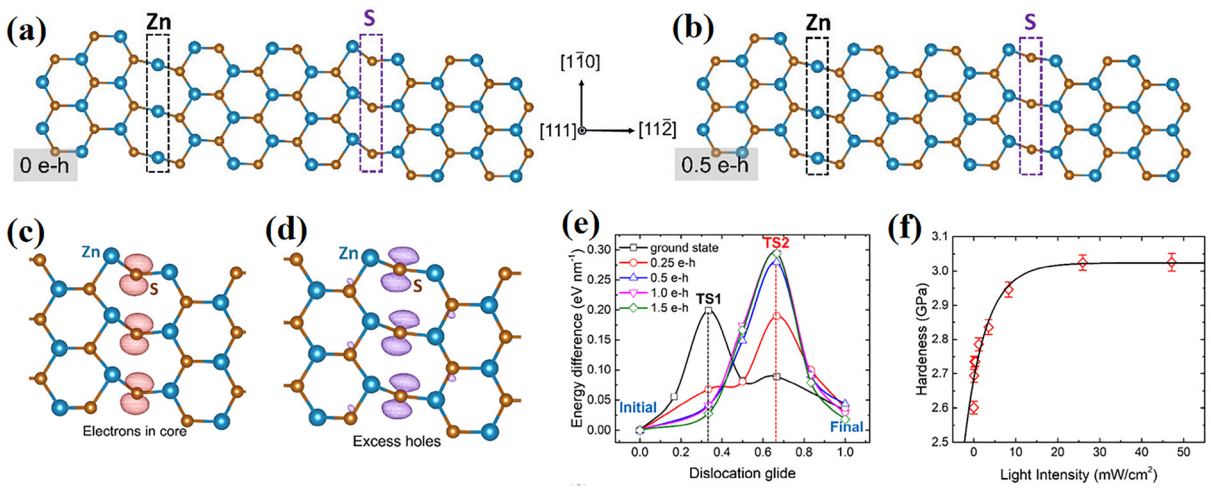

Fig. 6 Atomistic structures of the 30° Zn-core and S-core partial dislocations in ZnS under different carrier concentrations. (a) DFT-relaxed configuration of the dislocation dipole in the ground state (0 e–h), showing the characteristic Zn-core (black box) and S-core (purple box) units. (b) Corresponding structure under photoexcitation (0.5 e–h), where injected carriers induce noticeable geometric straightening around the S-core, while the Zn-core remains comparatively unchanged. (c) Band-decomposed charge density at the ground state (0 e–h), showing electrons localized at the S-core defect states. (d) Charge-density difference induced by photoexcitation (0.5 e–h), illustrating the accumulation of excess holes at the S-core region and the corresponding redistribution along nearby Zn–S bonds. (e) Calculated energy profiles along the dislocation glide path for the 30° S-core in the ground state and under different carrier concentrations (0.25–1.5 e–h). The introduction of photoexcited carriers progressively elevates the energy barriers at TS1 and TS2, indicating a light-induced increase in the Peierls stress. (f) Measured hardness of ZnS as a function of illumination intensity, showing a rapid hardening at low light flux followed by saturation, consistent with the computationally predicted increase-and-plateau behavior of the glide barrier.[87] Figures are reproduced from ref. 87 under the terms of the Creative Commons CC BY 4.0 license.

Using ML-FF trained on constrained-excitation DFT data, they constructed quadrupolar edge-dislocation dipoles in triclinic supercells, fixing the dislocation line along [110] for four periodic repeat units (~1.51 nm) and systematically enlarging the transverse cell dimensions (2L × L). This hierarchical approach enabled them to examine photoexcitation-dependent dislocation mobility at scales and levels of statistical sampling inaccessible to DFT alone.

Fig. 7 summarizes the structural and mechanical consequences of photoexcitation. Fig. 7(a) presents a comparison of the single-period (SP) and double-period (DP1/DP2) core configurations of 30° and 90° partial dislocations in the ground state (GS) and excited state (ES). Across all characters, the same core topologies remain energetically preferred in ES as in GS. The median bond lengths shift by only a few 10^{-3} Å, and the overall bond-length distributions nearly overlap, demonstrating that photoexcitation does not induce major core reconstructions or markedly stiffen/soften individual bonds for either the Zn-core or S-core partials. Contrarily, Fig. 7(b) shows that Peierls stresses substantially increase under excitation: from ≈1.3 to ≈1.6 GPa for the 30° S-core, ≈1.8 to ≈2.9 GPa for the 30° Zn-core, ≈2.2 to ≈2.4 GPa for the 90° S-core and ≈0.9 to ≈1.4 GPa for the 90° Zn-core, corresponding to roughly 10%–60% enhancements depending on dislocation character. Fig. 7(c) presents the essentially unchanged bond-length statistics, showing that the primary effect of photoexcitation is not local bond hardening but rather a redistribution of shear, charge density, and local electrostatic interactions around the dislocation cores. This redistribution increases the lattice resistance encountered by the entire dislocation line, thereby elevating the Peierls barrier and reducing mobility. Luo *et al.*'s study demonstrates that even when individual core bonds change only subtly, the collective electronic and elastic responses of the dislocation line can be strongly modified by photoexcitation—a crucial insight only accessible through DFT-informed, large-scale ML-FF simulations.

2.4. Extending to other II–VI semiconductors (ZnO, CdTe, *etc.*): sign change and defect chemistry

2.4.1. ZnO. In ZnS, we have observed that band-gap illumination modifies the charge states of native defects and thereby alters the electrostatic pinning landscape experienced by charged dislocations, resulting in light-controlled changes in flow stress. A natural question is whether this defect-charging–dislocation-pinning mechanism is unique to cubic ZnS or represents a broader characteristic of II–VI semiconductors, including wurtzite oxides such as ZnO. The progression of ZnO photoplasticity studies over the past decades—ranging from early bulk compression tests to modern photoindentation experiments on orientation-selected crystals—strongly supports the latter view and elucidates how the photoplastic response depends on slip system, carrier dynamics, and deformation length scale.

The first evidence came from the classic work by Carlsson and Svensson, who compressed vapor-grown n-type ZnO crystals and found that switching on above-gap illumination during reloading reproducibly increased the flow stress by ~30%.[1] The strengthening increased with light intensity and reached saturation at high photon flux, with a spectral maximum near the band gap of ZnO (~3.2 eV). The effect persisted for 10–15 s after the light was turned off. They attributed this behavior to the photo-ionization of excess Zn donors ($Zn^{+} \rightarrow Zn^{2+}$), which more strongly interact with negatively charged dislocations and thereby elevate the stress required for glide through enhanced dislocation locking.

Modern photoindentation studies have refined this picture by resolving how illumination influences dislocation activity beneath an indenter. Li[89] and co-workers developed a (0001) 45° off-axis ZnO crystal to preferentially activate basal slip and performed nanoindentation under dark and near-band-edge illumination. Their results indicate that illumination primarily suppresses post-yield plasticity: elastoplastic stress fields

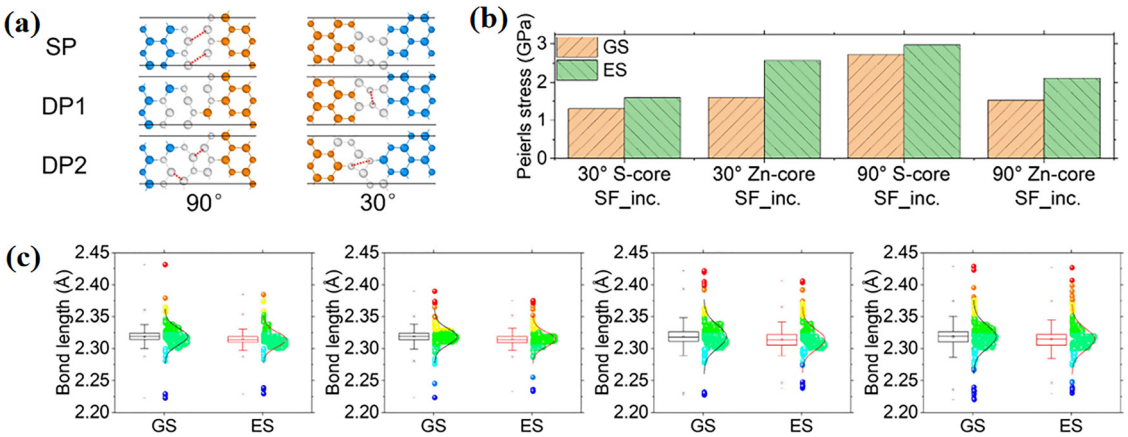

Fig. 7 (a) Atomic models of single-period (SP) and double-period (DP1/DP2) reconstructions for 90° and 30° partial dislocations. Blue and orange spheres denote the Zn and S atoms, respectively. Red dashed lines represent regions of possible Coulomb repulsion between atoms, indicating the geometric and chemical driving forces behind the different reconstruction motifs. (b) Summary of Peierls stress at GS and ES for all four partial dislocations. (c) Structural representation with color-coded chemical bonds based on the bond-length distribution data.[88] Copyright is from the American Chemical Society, ACS Materials Letters.[88]

extracted from pop-in and creep segments indicate that the dislocation motion ceases at a higher stress under illumination than in darkness. This behavior is consistent with an elevated Peierls barrier for basal dislocations due to carrier trapping and subtle core reconstruction. Based on this finding, Oguri *et al.*[18] applied the same photoindentation methodology to the (0001) c-plane ZnO at low loads, where only pyramidal slip is activated. They found that the maximum shear stress at the first pop-in event is essentially insensitive to 405-nm illumination, indicating that homogeneous nucleation is not strongly affected by light. Contrarily, nanoindentation creep is reduced by ~28%, and TEM cross-sections show shallower and fewer pyramidal slip bands under illumination – direct evidence indicating that glide mobility, rather than nucleation, is the dominant light-sensitive component.

Collectively, these three experiments establish a coherent picture: in wurtzite ZnO, illumination consistently suppresses the dislocation glide across basal and pyramidal slip systems while maintaining the nucleation threshold. This suppression arises from interactions between photoexcited carriers and dislocation cores, which modify local electrostatic and structural environments and increase resistance to dislocation motion. Therefore, ZnO not only echoes photoplastic strengthening observed in ZnS but also demonstrates that the underlying carrier–dislocation coupling is robust across crystal structures, slip systems, and length scales.

2.4.2. CdTe. Among the II–VI semiconductors, CdTe displays an unusually rich and non-monotonic photomechanical response: illumination can either harden or soften the crystal. In their seminal study, Gutmanas *et al.*[90] showed that positive and negative photoplastic effects can occur in the same CdTe crystal, with the sign of the effect switching depending on the doping type, deformation history, thermal treatment, and illumination intensity. Their study demonstrated that plastic deformation, prior dislocation activity, and increasing carrier density can promote a transition from illumination-induced hardening to softening.

This bipolar behavior distinguishes CdTe from other materials such as ZnS or ZnSe, where the illumination effects are generally unidirectional. Furthermore, it suggests that the dislocation mobility in CdTe is governed by a competition between carrier trapping, interaction with local obstacles, thermal activation, and, in certain regimes, double-kink nucleation. Consequently, CdTe represents a critical case study for understanding how optical excitation can modulate dislocation motion in fundamentally different ways, providing essential insights for extending photoplasticity concepts beyond more ionic systems.

Building on this experimental picture, Luo *et al.*[52] used ML-FFs to resolve, at the atomic scale, how excitation controls dislocation mechanics in CdTe. They developed ML-FF models for the ground state and two excited states with distinct carrier concentrations, achieving accuracies of a few meV per atom in energy and better than 7% in elastic moduli. This level of accuracy enabled large-scale molecular dynamics simulations of supercells containing quadrupolar dipoles of 30° and 90° partial dislocations on {111} planes. This setup enabled the extraction of Peierls stresses from MD shear simulations with minimal finite-size effects (Fig. 8(a) and (b)).

The resulting core-structure analysis provides a mechanistic explanation for the dual photoplasticity of CdTe. Luo *et al.*[52] surveyed all the reported single-period (SP) and double-period (DP) reconstructions of Cd- and Te-core partials. They found that (1) Cd-core 30° and Te-core 90° partials retain the SP structure across all excitation levels; (2) Te-core 30° partials exhibit a bent Cd–Te–Cd chain in the ground state that partially straightens under illumination, effectively shifting an SP′ configuration back to SP; and (3) Cd-core 90° partials undergo substantial excitation-dependent reconstructions: DP1 → SP′ → DP′ from GS to ES0.5% to ES2% (Fig. 9(a)–(c)).

MD shear simulations along directions that increase (SF_inc.) or decrease (SF_dec.) the stacking fault show how these excitation-driven core reconstructions influence macroscopic mechanical response. SF_inc. shearing often produces strong nonlinearity and even an FCC → BCC martensitic transformation in the Cd sublattice, whereas SF_dec. shearing remains nearly elastic until the Peierls stress is reached. From Fig. 8(g), (h), Luo *et al.* extracted the Peierls stresses for all four partials. The minimum Peierls stress initially increases by ~21% at ES0.5% compared with the ground state and then decreases by ~38% between ES0.5% and ES2%, ultimately ending ~24% below the ground-state value at ES2%. This non-monotonic evolution reflects the experimentally observed transition from positive photoplasticity at moderate excitation to negative photoplasticity at high excitation: modest carrier densities stiffen specific core structures and harden the crystal, whereas higher excitation promotes alternative glide paths and local phase transformations that re-soften it.

2.5. Summary: photoplasticity in ionic semiconductors

Across ZnS, ZnO, CdTe, and other II–VI semiconductors, a coherent picture has emerged: illumination generally strengthens ionic materials by suppressing dislocation glide. Experiments spanning macroscopic compression, micro-pillar testing, and photo-nanoindentation consistently show increases in flow stress, hardness, and creep resistance under near-band-edge illumination, often accompanied by a transition in deformation mode—from conventional dislocation glide in darkness to twinning or cleavage under illumination. Atomistic studies using DFT, constrained DFT and ML-FF provide a unifying explanation. In strongly ionic compounds, such as ZnS and ZnO, photoexcited holes preferentially localize at S-rich dislocation cores, driving Zn–S bond rearrangements that elevate the Peierls barrier and reduce glide mobility; photoelectrons on cation-rich cores play only a minor role. CdTe, with its lower ionicity and narrower band gap, occupies a transitional regime in which the same carrier–core interactions can either increase or decrease glide resistance, producing a crossover from light-induced hardening to softening depending on the excitation level. Collectively, these findings indicate that photoplasticity in ionic semiconductors is fundamentally a charge-controlled phenomenon. Wide band gaps, deep defect states, and strongly polarized dislocation cores make their

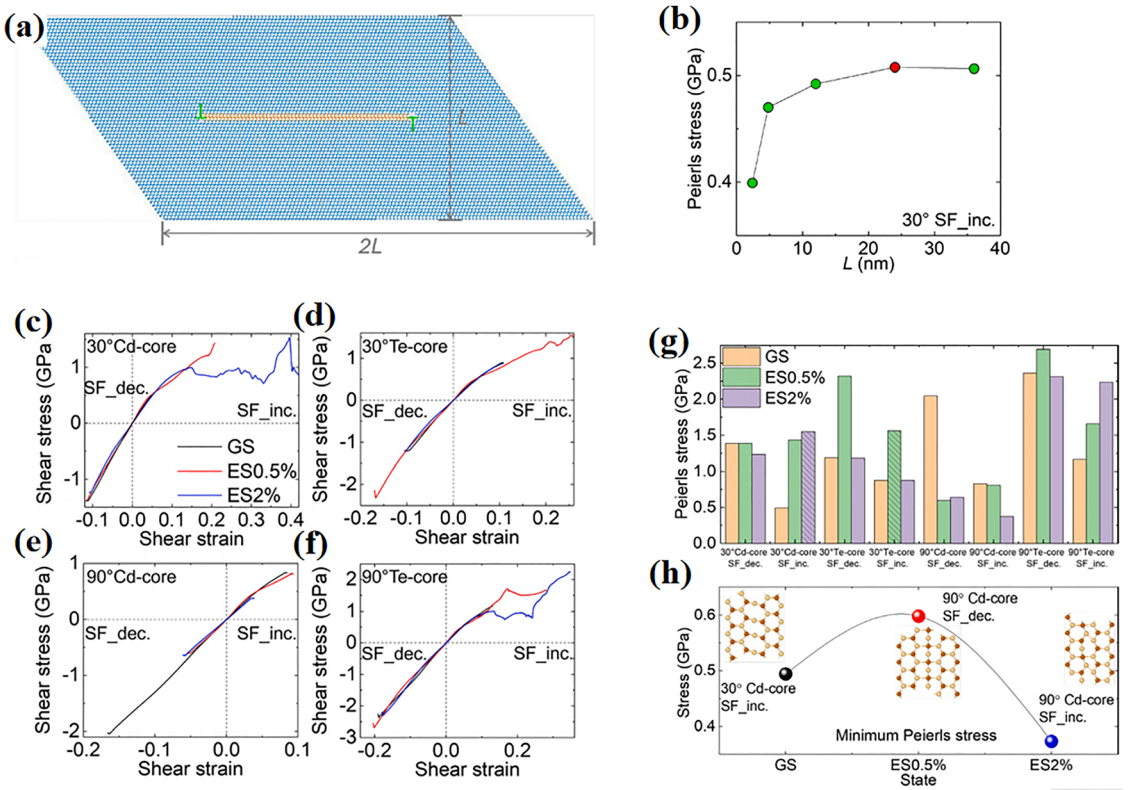

Fig. 8 (a) Large triclinic supercell used for CdTe dislocation simulations, containing a quadrupolar partial-dislocation dipole under full periodic boundary conditions. (b) Convergence of the Peierls stress of the 30° Cd-core partial dislocation as a function of model size LLL, showing stable values beyond ~20 nm. (c–f) Stress–strain curves for 30° Cd-core, 30° Te-core, 90° Cd-core, and 90° Te-core partials, respectively, under shear directions that increase (SF_{inc}) or decrease (SF_{dec}) the stacking fault. These curves are used to extract the Peierls stresses in each electronic state. (g) Peierls stresses of all 30° and 90° Cd- and Te-core partial dislocations in CdTe under the ground state (GS) and excited states (ES0.5%, ES2%). Hatched bars denote lower bounds where no dislocation motion was observed. (h) Minimum Peierls stress *versus* photoexcitation level the transition from strengthening (ES0.5%) to softening (ES2%). Insets show representative core structures corresponding to the identified minima.[52] Copyright is from Elsevier, International Journal of Mechanical Sciences.[52]

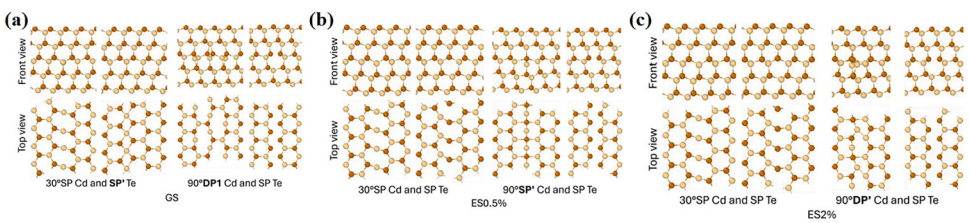

Fig. 9 (a–c) Stable core structures of 30° and 90° Cd- and Te-core partial dislocations in CdTe under different excitation states: (b) ground state (GS), (c) ES0.5%, and (d) ES2%. Front- and top-view configurations are shown for each dislocation type. Cd and Te atoms are represented by yellow and orange spheres, respectively.[52] Copyright is from Elsevier, International Journal of Mechanical Sciences.[52]

plasticity exceptionally sensitive to carrier redistribution under illumination. This behavior establishes a clear mechanistic baseline against which contrasting photoplastic responses of covalent semiconductors can be understood.

3. Photoplasticity in covalent semiconductors

In contrast to the ionic II–VI compounds discussed in Section 2, covalent semiconductors such as GaP, GaAs, Si, and Ge often exhibit the opposite trend: under near-band-edge illumination, they soften rather than harden, with reduced yield stress, enhanced creep, and diminished work hardening.[2,4,21–23,83–88] This sign reversal can be traced to several key features of covalent bonding and defect chemistry: (i) strongly directional sp^3 bonds and less ionic dislocation cores, which prevent large quasi-static line charges from building up as in ZnS or ZnO; (ii) longer carrier lifetimes and relatively shallow native defects, so that photoexcited carriers are efficiently captured at core-related levels where non-radiative recombination locally weakens bonds and assists kink formation;[91–95] (iii) carrier

screening of the residual core charge, which reduces long-range Coulomb fields and reduces the effective Peierls stress.[96–99] Collectively, these factors make III–V and group-IV semiconductors natural hosts for negative photoplasticity, providing a covalent counterpart to the light-induced hardening of ionic II–VI crystals.

This section summarizes how experiments and computational studies consistently demonstrate that covalent semiconductors respond to illumination through carrier-mediated bond weakening rather than core charging, providing a mechanistic basis for the light-induced softening trends discussed in the following subsections.

3.1. Historical observations in III–V and group-IV crystals

Previous studies on group-IV semiconductors, such as Si and Ge, reported that near–band-edge illumination could produce slight enhancements in dislocation motion, but only within a very shallow surface region.[100–102] Therefore, the resulting softening observed during indentation was attributed to surface band-bending effects and changes in dislocation charge and was viewed as a surface-localized photomechanical response rather than genuine bulk photoplasticity. A more definitive picture of photoplasticity emerged from early work on III–V semiconductors, particularly GaX (X = P or As).[2,4,20–22,103] Indentation, etch-pit analysis, and microscopy studies demonstrated that illumination can substantially enhance the mobility of specific dislocation segments, resulting in noticeable reductions in flow stress—a clear case of negative photoplasticity. These findings firmly established that carrier–dislocation interactions can promote rather than suppress dislocation glide in covalent semiconductors, contrary to the illumination-induced hardening characteristic of more ionic II–VI materials, such as ZnS. Collectively, these historical observations showed that negative photoplasticity is strongly governed by bonding character, carrier localization behavior, and defect chemistry, providing the conceptual foundation for modern theoretical and atomistic investigations into light-modulated plasticity in covalent semiconductors.

3.2. GaX as a prototype of negative photoplasticity

The first systematic evidence of negative photoplasticity in III–V semiconductors came from Maeda's 1977 study of GaP single crystals.[4] Using Vickers micro-indentation on P$\{\bar{1}\bar{1}\bar{1}\}$ surfaces, they analysed dislocation rosette patterns and quantified the motion of the leading Ga-edge dislocation by its radial displacement L. Under visible illumination during indentation, L markedly increased in n- and p-type GaP, with a stronger effect in n-type crystals, demonstrating that light enhances dislocation mobility rather than suppressing it. The photomechanical softening was observable only below ~230 °C, and at 155 °C, the increase in L caused by light was equivalent to a ~40 °C increase in test temperature in darkness (Fig. 10(a)). The effect persisted over a broad spectral range on both sides of the fundamental absorption edge, consistent with a surface-type mechanism controlled by band bending and the charge state of α-type dislocations.

Later, Mdivanyan and Shikhsaidov reported the first bulk-negative photoplastic effect in GaAs under uniaxial compression and four-point bending.[22] In pre-deformed n- and p-type crystals, illumination during low-temperature (120 °C–250 °C) deformation reduced the plastic flow stress and yield point (Fig. 10(b)), with the stress–strain curves reversibly returning to the dark level when the light was switched off. Negative photoplasticity was confined to $T \lesssim 300$ °C, and its magnitude peaked when the excitation wavelength (~900 nm) matched the GaAs band gap (Fig. 10(c)). They further measured dislocation velocities using a double-etching technique and found that illumination increases the velocity by nearly an order of magnitude at low shear stresses and reduces the activation energy from ~0.9 eV in darkness to ~0.3 eV, consistent with a recombination-enhanced dislocation glide mechanism.

A major conceptual breakthrough occurred in 1989–1990, when Depraetère *et al.* established a mechanistic framework directly linking light-enhanced dislocation motion to non-radiative electron–hole recombination at dislocation-related defect levels.[20] Microhardness rosette experiments at room temperature revealed that laser illumination selectively activates dislocation glide along the (110) planes. In n-type and semi-insulating GaAs, both orthogonal (110) glide directions were photoactivated, producing symmetric rosette arms (Fig. 11(a) and (b)). In contrast, p-type GaAs exhibited a photoactivated glide in only one (110) direction (Fig. 11(c)), demonstrating a strong doping dependence.

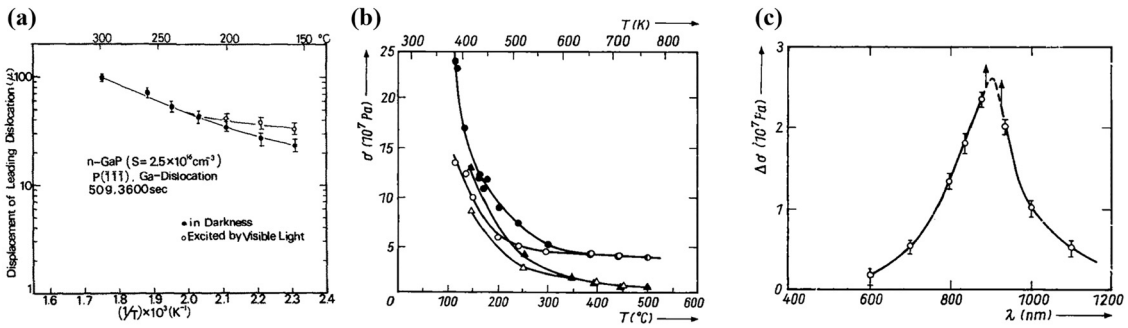

Fig. 10 (a) Temperature dependence of the radial displacement L of the leading Ga-edge dislocation in n-type GaP under indentation on the P$\{\bar{1}\bar{1}\bar{1}\}$ surface. (b) Yield point (σ_y) of n- and p-type GaAs crystals as a function of temperature under compressive deformation. (c) Spectral dependence of the illumination-induced stress reduction ($\Delta\sigma$) in GaAs.[22] Copyright is from Wiley, Physica Status Solidi (a).[22]

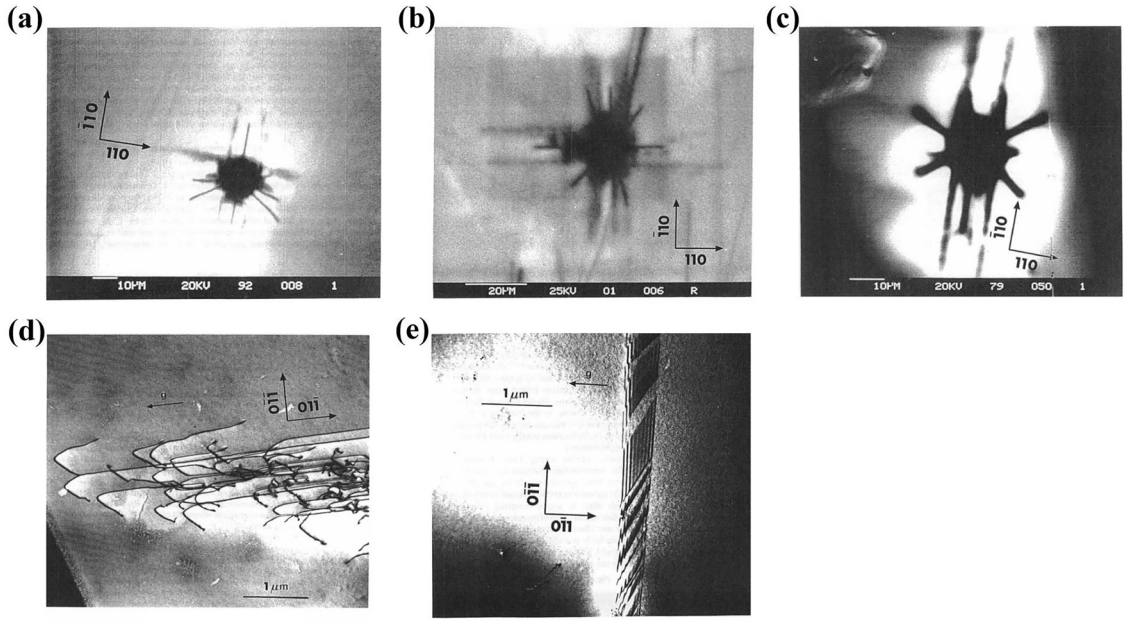

Fig. 11 Cathodoluminescence images of photo-developed micro-indentations in GaAs with varying doping types. Under above-band-gap illumination, n-type (a) and semi-insulating (b) crystals exhibit symmetric rosette patterns with arms extending along the two orthogonal ⟨110⟩ glide directions. In contrast, p-type GaAs (c) shows pronounced arm development only along the β glide direction, while the orthogonal ⟨110⟩ direction remains inactive. (d and e) TEM images of the microhardness rosette arms formed under illumination in n-type GaAs. The two orthogonal ⟨110⟩ directions exhibit distinctly different dislocation substructures.[20] Copyright is from Taylor & Francis Groups, Philosophical Magazine A.[20]

TEM observations showed that illuminated rosettes consisted of long screw segments in one (110) direction and partial dislocations with large stacking faults in the orthogonal direction (Fig. 11(d) and(e)), suggesting that photoactivation affects not only nucleation but also kink propagation along the dislocation line. Complementary studies of degradation in GaAs/GaAlAs heterostructures demonstrated that dark-line defects (DLDs) first appear along a single (110) direction and only later extend to (100). Notably, degradation occurred only under above-band-gap illumination, confirming that carrier generation and recombination, rather than purely optical absorption or heating, promote the photoplastic response. To elucidate these findings, the authors proposed two dislocation-related recombination centers: B1 (associated with As-core dislocations) and B2 (associated with Ga-core dislocations). Configuration-coordinate analysis revealed that the non-radiative recombination at these centers injects energy into the dislocation line, lowering the activation barrier for double-kink formation and thereby enhancing glide. The distinct recombination pathways also explain the doping selectivity: B1-mediated glide is active only in n-type GaAs, whereas B2 centers enable photoactivation in n- and p-type crystals. This body of work provided the first physically consistent microscopic model for photoplasticity in GaAs, identifying recombination-enhanced kink nucleation as the main mechanism.

From Maeda's early study[4] on GaP to subsequent Vickers[104] and TEM studies on GaAs, and finally to device-level degradation experiments in AlGaAs/GaAs[103] laser structures, a consistent picture of negative photoplasticity in covalent III–V semiconductors has emerged. Vickers microhardness tests on bulk GaAs under low loads showed that near-band-edge infrared illumination ($\lambda \approx 900$–940 nm) reduces hardness by about 15–25% compared with darkness, whereas high loads largely mask the effect owing to strong work hardening. TEM observations of the corresponding rosettes showed that the [110] arms, mainly composed of α-type total dislocations, become considerably longer under illumination, whereas the orthogonal [1$\bar{1}$0] (β-type) arms and associated twins are only weakly affected. These data establish that light selectively enhances α-dislocation mobility and that the magnitude of softening follows the spectral response of the earlier flow-stress NPPE, peaking near the GaAs band gap.

GaP offers a complementary and, in some respects, more detailed prototype. In Maeda's indentation study, the radial displacement L of the leading Ga-edge dislocation, extracted from rosette patterns, reported that α-type dislocations were consistently more mobile than β-type and that n-type crystals exhibited larger L values than p-type under equivalent conditions. Visible illumination increased L and accelerated rosette growth in doping types, confirming a true light-induced softening rather than any form of illumination-driven hardening. The effect persisted for wavelengths above and below the absorption edge and peaked near the band gap, suggesting that enhanced dislocation glide is responsible, not heating.

Device-scale experiments on AlGaAs/GaAs double heterostructures closed this phenomenological loop. In laser-like structures, intense above-band-gap illumination generates dark-line defects (DLDs) that elongate initially along the ⟨110⟩ (glide-controlled) and later along the ⟨100⟩ (climb-controlled) directions in the GaAs active layer, directly linking photoactivated

glide to the initial stages of laser degradation. Low-temperature cathodoluminescence mapping shows local Al-content fluctuations in the upper AlGaAs cladding. The resulting stress variations, on the order of 1 MPa, are sufficient to induce photo-activated dislocation glide. By comparing the elastic limits in dark and illuminated conditions, the non-radiative recombination energy driving this glide was inferred to be ~0.9 eV, consistent with transitions at defect levels associated with reconstructed dislocation cores rather than intrinsic dislocation states.

Collectively, these bulk, microhardness, and device-level studies demonstrate that the negative photoplasticity in GaX materials is a robust, carrier-mediated softening phenomenon that preferentially enhances α-dislocation glide and that it operates not only in ideal single crystals but also under realistic operating conditions in optoelectronic devices.

A recent first-principles study by Hoshino *et al.*[105] provided a microscopic mechanism for negative photoplasticity in GaP by explicitly tracking how excess carriers modify 30° Shockley partial-dislocation cores. They model a dissociated partial pair on a polar {111} plane so that one core is Ga-rich and the other is P-rich. In the neutral state, both cores undergo a double-period reconstruction, forming Ga–Ga or P–P bonds along the line. The introduction of excess electrons or holes—mimicking carrier injection under illumination—fundamentally alters this balance. Formation-energy diagrams as a function of Fermi level (Fig. 12(a)) show that electrons preferentially localize at the P-rich core, whereas holes localize at the Ga-rich core. Local DOS and charge-density maps (Fig. 12(b)–(d)) show that this localization destabilizes the like-atom bonds responsible for the reconstructed structure. Consequently, the lowest-energy configuration switches from "reconstructed–reconstructed" to mixed states with one reconstructed and one unreconstructed core on the carrier-rich dislocation segment.

To connect this structural change with mechanical behavior, the authors estimated simplified Peierls barriers (Fig. 12(e)) using nudged-elastic-band calculations. In the neutral state, the Ga- and P-core partials show barrier heights $\Delta E_P \approx 2$ eV nm^{-1}. Under excess-carrier conditions, the glide barrier for the carrier-rich core lowers to less than half this value, whereas the opposite core is only weakly affected. Thus, illumination induces a local core transformation from reconstructed to unreconstructed, substantially lowering the glide barrier and selectively accelerating the motion of the carrier-decorated dislocation segments. This atomistic mechanism provides a direct explanation of the experimentally observed increase in dislocation mobility in illuminated GaP and establishes a clear association between macroscopic negative photoplasticity and carrier-controlled reconstructions of dislocation cores.

3.3. Summary: photoplasticity in covalent semiconductors

In covalent III–V and group-IV semiconductors, photoplasticity often demonstrates the opposite sign of that observed in ionic II–VI compounds: illumination typically softens the crystal and enhances dislocation mobility. Historical studies on GaP and GaAs, followed by subsequent study on Ge and Si, consistently

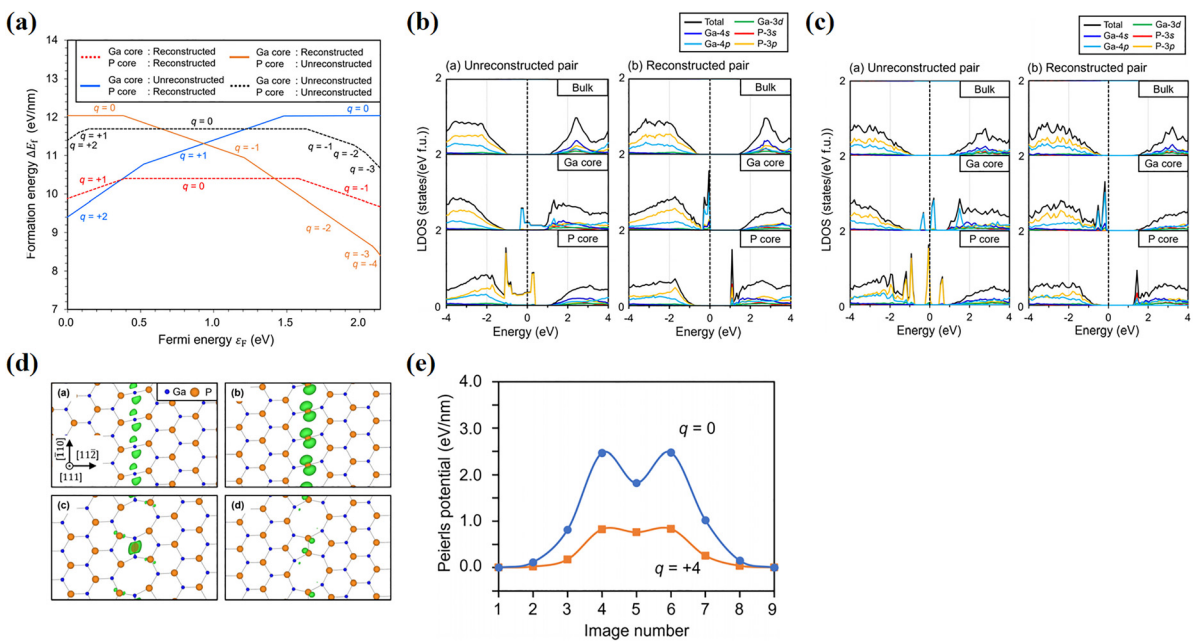

Fig. 12 (a) Formation-energy change ($\Delta E_f(q)$) *versus* Fermi level (ε_F) from GGA+*U* calculations for 288- and 576-atom supercells, comparing unreconstructed, reconstructed, and mixed partial-dislocation core pairs. LDOS of (b) unreconstructed and (c) reconstructed partial-dislocation pairs with $q = 0$ $q = 0$ $q = 0$ from GGA+*U* calculations. Bulk LDOS is shown in the top panels for comparison. The vertical dashed lines indicate the highest occupied levels. (d) Band-decomposed charge densities of defect-induced states for the partial-dislocation cores with $q = 0$: (a) Ga-core and (b) P-core configurations in the unreconstructed pair and (c) Ga-core and (d) P-core configurations in the reconstructed pair. (e) Peierls potentials of the Ga-core 30° partial dislocation in the neutral and charged ($q = +4$) states obtained from NEB calculations. Images 1 and 9 correspond to the stable positions on the slip plane, with the potential of image 1 set to zero.[105] Copyright is from American Physical Society, Physical Review Materials.[105]

showed reductions in yield stress, accelerated creep, and suppressed work hardening—phenomena collectively termed negative photoplasticity. These behaviors can be rationalized by considering how directional covalent bonding, less highly charged dislocation cores, and longer carrier lifetimes modify carrier–dislocation interactions. In such materials, photoexcited carriers can screen long-range elastic fields, promote local core reconstructions, or participate in non-radiative recombination processes that decreases the activation energy for glide and kink nucleation. Recent atomistic simulations on GaP- and GaAs-type systems have begun linking these macroscopic trends to illumination-induced changes in generalized stacking-fault energies and core bonding configurations. However, compared with ionic semiconductors, the photoplastic response in covalent materials is more sensitive to doping, defect chemistry, and recombination kinetics, and genuine bulk photoplasticity is harder to separate from surface or contact effects.

Collectively, these results indicate that the same basic ingredients—carrier injection, core charging, and carrier-assisted structural rearrangements—can invert the sign of photoplasticity when embedded within a different bonding and defect landscape. This contrast highlights the need for a unified framework capable of describing carrier–dislocation interactions across ionic and covalent limits.

4. Summary and outlook

This review has traced how illumination modifies plasticity in inorganic semiconductors *via* direct coupling to dislocation cores. In ionic II–VI systems (ZnS, ZnO, CdTe, *etc.*), a consistent positive photoplasticity picture emerges: near-band-gap light generally increases flow stress and hardness, suppresses creep, and shortens glide distances. Atomistic simulations show that photoexcited carriers localize at charged partial cores, promote core reconstructions, and strengthen key bonds, thereby elevating Peierls barriers. ZnS and ZnO exemplify this carrier-trapping–induced hardening; CdTe is a borderline case where competing core states can result in either hardening or softening, depending on conditions. In covalent III–V and group-IV crystals, illumination instead tends to enhance dislocation mobility. Classic GaP/GaAs experiments and subsequent study on Ge/Si revealed reductions in yield stress, enhanced glide, and modified work hardening under illumination. Early models highlight carrier-assisted kink nucleation and drag reduction. Recent first-principles and core-structure studies indicate that changes in generalized stacking-fault energies and covalent bonding under excitation can lower the effective glide barrier. Collectively, the ionic and covalent cases illustrate that photoplasticity is not a single phenomenon but rather the outcome of a balance between bonding character, core charge state, and carrier generation–recombination kinetics. Essentially, light injects carriers that can either pinch the dislocation (if they charge it) or lubricate it (if they break bonds or screen fields), with the material's chemistry dictating which dominates.

From an application standpoint, it is noteworthy that most optoelectronic devices employ semiconductors in thin-film form rather than as bulk crystals. In such confined geometries, interfaces, residual stresses, substrate constraints, and size effects can substantially modify dislocation activity and plastic deformation pathways. Consequently, photoplastic responses in semiconducting thin films may quantitatively or even qualitatively differ from those observed in bulk materials. Therefore, understanding how illumination interacts with dislocations, interfaces, and stress states in thin films is essential for translating fundamental photoplastic mechanisms into flexible and wearable optoelectronic technologies.

Beyond single crystals, many technologically relevant semiconductors are polycrystalline or amorphous, where grain boundaries, structural disorder, and defect states dominate mechanical behavior. These systems are often highly responsive to illumination, including sub-band-gap excitation, owing to their high-density localized electronic states.[106,107] In this broader context, van der Waals semiconductors, particularly in their two-dimensional form, have also emerged as an active research platform for light-induced mechanical phenomena, although their underlying physics often differs from bulk dislocation-mediated photoplasticity. How photogenerated carriers interact with grain boundaries, amorphous networks, low-dimensional structures, and defect complexes to influence plastic deformation remains largely unexplored and represents an important direction for future research. In the future, several promising avenues could advance this field: (1) unified dislocation core–charge framework. Systematic DFT/constrained DFT/ML studies treating ionic and covalent materials on equal footing—mapping Peierls barriers, core reconstructions, and carrier localization as functions of Fermi level and excitation density—are warranted to distill general design rules for "photomechanical band-engineering." (2) Advanced *in situ* experiments. Further development of photo-mechanical testing methods (nanoindentation, micropillar compression, *in situ* TEM with illumination) can isolate photoplastic effects from thermal/artifact effects. Time-resolved techniques can probe carrier–dislocation dynamics and after-effects. (3) Defect engineering. As native and intentional defects mediate photoplasticity, tailoring defect chemistry (dopants, vacancies) provides a route to amplify or switch photoplastic responses. For example, the introduction of deep-level dopants may provide stronger light-induced pinning or release of dislocations. (4) Device-level implications. Investigation of photoplasticity in actual device materials (*e.g.* LED structures, power electronics, and thin-film heterostructures) under operating conditions can reveal its impact on reliability. Controlled illumination can be employed for on-the-fly stress relief or strengthening in devices and during fabrication. We hope that this review will guide the rational design and utilization of light-tunable mechanics in semiconductors, bridging fundamental insights with practical applications.

Author contributions

C. Cao: data curation, investigation, validation, and writing – original draft. Q. An: conceptualization, funding acquisition,

resources, supervision, writing – original draft, and writing – review and editing.

Conflicts of interest

There are no conflicts to declare.

Data availability

No primary research results, software or code have been included, and no new data were generated or analyzed as part of this review.

Acknowledgements

This work was supported by the National Science Foundation (NSF) with funding number 2347218 and the U.S. Department of Energy (DOE) Office of Science with funding number DE-SC0026363.

References

1 L. Carlsson and C. Svensson, *Solid State Commun.*, 1969, **7**, 177–179.
2 S. Koubaiti, J. J. Couderc, C. Levade and G. Vanderschaeve, *Mater. Sci. Eng. A*, 1997, **234**, 865–868.
3 V. F. Mayer and J. M. Galligan, *Appl. Phys. Lett.*, 1982, **40**, 1020–1021.
4 K. Maeda, O. Ueda, Y. Murayama and K. Sakamoto, *J. Phys. Chem. Solids*, 1977, **38**, 1173–1179.
5 L. Carlsson and C. Svensson, *J. Appl. Phys.*, 1970, **41**, 1652–1656.
6 G. C. Kuczynski and R. F. Hochman, *Phys. Rev.*, 1957, **108**, 946.
7 L. Carlsson and C. N. Ahlquist, *J. Appl. Phys.*, 1972, **43**, 2529–2536.
8 M. Li, K. Luo, X. Ma, B. Kumral, P. Gao, T. Filleter, Q. An and Y. Zou, *arXiv*, 2025, preprint, arXiv:2503.19189, DOI: 10.48550/arXiv.2503.19189.
9 Y. Oshima, A. Nakamura and K. Matsunaga, *Science*, 2018, **360**, 772–774.
10 C. N. Ahlquist, M. J. Carroll and P. Stroempl, *J. Phys. Chem. Solids*, 1972, **33**, 337–342.
11 Y. A. Osip'yan and V. F. Petrenko, *Sov. Phys. JETP*, 1973, **36**, 916–920.
12 X. J. Zheng, G. C. Yu, Y. Q. Chen, S. X. Mao and T. Zhang, *J. Appl. Phys.*, 2010, **108**, 094305.
13 S. Aftergut, J. J. Bartfai and B. C. Wagner, *Appl. Opt.*, 1969, **8**, 161–165.
14 T. J. Garosshen, C. S. Kim and J. M. Galligan, *Appl. Phys. Lett.*, 1990, **56**, 335–336.
15 A. H. Durgaryan, H. S. Melkonyan and R. P. Vardapetyan, *Solid State Commun.*, 1990, **73**, 185–189.
16 J. Pellegrino and J. M. Galligan, *Phys. Status Solidi A*, 1988, **110**, 565–573.
17 Y. Ohno, T. Taishi and I. Yonenaga, *Phys. Status Solidi A*, 2009, **206**, 1904–1911.
18 H. Oguri, Y. Li, E. Tochigi, X. Fang, K. Tanigaki, Y. Ogura, K. Matsunaga and A. Nakamura, *J. Eur. Ceram. Soc.*, 2024, **44**, 1301–1305.
19 P. Horvath, S. B. Sadale, M. Suchea, S. Christoulakis, R. Voicu, C. Tibeica, I. Bineva, R. Muller, T. Kitsopoulos and G. Kiriakidis, *Sens. Lett.*, 2008, **6**, 558–563.
20 E. Depraetère, D. Vignaud, J. L. Farvacque, B. Sieber and A. Lefebvre, *Philos. Mag. A*, 1990, **61**, 893–907.
21 J. L. Farvacque, D. Vignaud, E. Depraetere, B. Sieber and A. Lefebvre, *Structure and Properties of Dislocations in Semiconductors 1989*, 1989, vol. 141.
22 B. E. Mdivanyan and M. S. Shikhsaidov, *Phys. Status Solidi A*, 1988, **107**, 131–140.
23 A. Polman, M. Knight, E. C. Garnett, B. Ehrler and W. C. Sinke, *Science*, 2016, **352**, aad4424.
24 B. Parida, S. Iniyan and R. Goic, *Renewable Sustainable Energy Rev.*, 2011, **15**, 1625–1636.
25 A. W. Hains, Z. Liang, M. A. Woodhouse and B. A. Gregg, *Chem. Rev.*, 2010, **110**, 6689–6735.
26 M. Bosi and C. Pelosi, *Prog. Photovoltaics Res. Appl.*, 2007, **15**, 51–68.
27 J. F. Geisz and D. J. Friedman, *Semicond. Sci. Technol.*, 2002, **17**, 769.
28 V. Avrutin, N. Izyumskaya and H. Morkoç, *Superlattices Microstruct.*, 2011, **49**, 337–364.
29 X. Menga, D. Zhangb, P. Fengb and N. Huc, *Renewable Energy*, 2021, **15**, 16.
30 J. B. Charpentier, T. Duigou, B. Chambion, P. Voarino and F. Chabuel, *Prog. Photovoltaics Res. Appl.*, 2023, **31**, 1428–1441.
31 J. Lee, J. Wu, M. Shi, J. Yoon, S.-I. Park, M. Li, Z. Liu, Y. Huang and J. A. Rogers, *Adv. Mater.*, 2011, **23**, 986.
32 M. Bilge, S. Ö. Kart, H. H. Kart and T. Cagin, *J. Achiev. Mater. Manuf. Eng.*, 2008, **31**, 29–34.
33 R. M. Martin, *Phys. Rev. B*, 1970, **1**, 4005.
34 C. A. Wolden, J. Kurtin, J. B. Baxter, I. Repins, S. E. Shaheen, J. T. Torvik, A. A. Rockett, V. M. Fthenakis and E. S. Aydil, *J. Vac. Sci. Technol., A*, 2011, **29**, 030801.
35 J. M. Pearce, *Renewable Energy*, 2008, **33**, 1101–1108.
36 V. F. Petrenko and R. W. Whitworth, *Philos. Mag. A*, 1980, **41**, 681–699.
37 G. Vanderschaeve, C. Levade and D. Caillard, *J. Microsc.*, 2001, **203**, 72–83.
38 C. P. Burger, *Exp. Mech.*, 1980, **20**, 381–389.
39 Y. A. Osip'Yan, V. F. Petrenko, A. V. Zaretskiĭ and R. W. Whitworth, *Adv. Phys.*, 1986, **35**, 115–188.
40 V. B. Shikin and Y. V. Shikina, *Phys.-Usp.*, 1995, **38**, 845.
41 J. H. You and H. T. Johnson, *Solid State Phys.*, 2009, **61**, 143–261.
42 C. C. Speake, P. J. Smith, T. R. Lomer and R. W. Whitworth, *Philos. Mag. A*, 1978, **38**, 603–606.
43 J. P. Hirth, J. Lothe and T. Mura, *J. Appl. Mech.*, 1983, **50**, 476–477.
44 H. Alexander and P. Haasen, *Solid state Physics*, Elsevier, 1969, vol. 22, pp. 27–158.

45 S. O. Valenzuela and M. Tinkham, *Nature*, 2006, **442**, 176–179.
46 F. Werner, *J. Appl. Phys.*, 2017, **122**, 135306.
47 T. Figielski, *Solid-State Electron.*, 1978, **21**, 1403–1412.
48 K. Maeda, K. Suzuki, M. Ichihara and S. Takeuchi, *J. Appl. Phys.*, 1984, **56**, 554–556.
49 C. Levade and G. Vanderschaeve, *J. Cryst. Grow.*, 1999, **197**, 565–570.
50 B. Wolf, A. Belger, D. C. Meyer and P. Paufler, *Phys. Status Solidi A*, 2001, **187**, 415–426.
51 G. Rivaud and J. C. Desoyer, *J. Phys. Colloq.*, 1983, **44**, C4–387.
52 K. Luo, R. Zhou and Q. An, *Int. J. Mech. Sci.*, 2025, **305**, 110765.
53 K. Nakagawa, K. Maeda and S. Takeuchi, *J. Phys. Soc. Jpn.*, 1981, **50**, 3040–3046.
54 J. Dong, Y. Li, Y. Zhou, A. Schwartzman, H. Xu, B. Azhar, J. Bennett, J. Li and R. Jaramillo, *Phys. Rev. Lett.*, 2022, **129**, 065501.
55 M. J. Klopfstein, D. A. Lucca and G. Cantwell, *Phys. Status Solidi A*, 2003, **196**, R1–R3.
56 S. C. Rai, K. Wang, Y. Ding, J. K. Marmon, M. Bhatt, Y. Zhang, W. Zhou and Z. L. Wang, *ACS Nano*, 2015, **9**, 6419–6427.
57 P. E. Lippens and M. Lannoo, *Phys. Rev. B: Condens. Matter Mater. Phys.*, 1989, **39**, 10935.
58 M. Oshikiri and F. Aryasetiawan, *Phys. Rev. B: Condens. Matter Mater. Phys.*, 1999, **60**, 10754.
59 M. Y. Nadeem and W. Ahmed, *Turk. J. Phys.*, 2000, **24**, 651–659.
60 B.-C. Shih, Y. Xue, P. Zhang, M. L. Cohen and S. G. Louie, *Phys. Rev. Lett.*, 2010, **105**, 146401.
61 X. Wang, J. Shi, Z. Feng, M. Li and C. Li, *Phys. Chem. Chem. Phys.*, 2011, **13**, 4715–4723.
62 F. Kurnia, Y. H. Ng, R. Amal, N. Valanoor and J. N. Hart, *Sol. Energy Mater. Sol. Cells*, 2016, **153**, 179–185.
63 Q. D. Ho and M. Castillo, *Comput. Mater. Sci.*, 2023, **216**, 111827.
64 D. Kurbatov, V. Kosyak, A. Opanasyuk and V. Melnik, *Phys. B*, 2009, **404**, 5002–5005.
65 J. B. Varley and V. Lordi, *Appl. Phys. Lett.*, 2013, **103**, 102103.
66 M. D. McCluskey and S. J. Jokela, *J. Appl. Phys.*, 2009, **106**, 071101.
67 L. Schmidt-Mende and J. L. MacManus-Driscoll, *Mater. Today*, 2007, **10**, 40–48.
68 F. Oba, M. Choi, A. Togo and I. Tanaka, *Sci. Technol. Adv. Mater.*, 2011, **12**, 034302.
69 D. M. Hofmann, D. Pfisterer, J. Sann, B. K. Meyer, R. Tena-Zaera, V. Munoz-Sanjose, T. Frank and G. Pensl, *Appl. Phys. A*, 2007, **88**, 147–151.
70 S. Kitou, Y. Oshima, A. Nakamura, K. Matsunaga and H. Sawa, *Acta Mater.*, 2023, **247**, 118738.
71 H. Oguri, Y. Li, X. Fang and A. Nakamura, *Appl. Phys. Lett.*, 2025, **126**, 114101.
72 K. Ishizuka and J. Taftø, *Struct. Sci.*, 1984, **40**, 332–337.
73 X. Meng, H. Xiao, X. Wen, W. A. Goddard Iii, S. Li and G. Qin, *Phys. Chem. Chem. Phys.*, 2013, **15**, 9531–9539.
74 O. Brafman, E. Alexander, B. S. Fraenkel, Z. H. Kalman and I. T. Steinberger, *J. Appl. Phys.*, 1964, **35**, 1855–1860.
75 M. De La Mata, R. R. Zamani, S. Martí-Sánchez, M. Eickhoff, Q. Xiong, A. Fontcuberta i Morral, P. Caroff and J. Arbiol, *Nano Lett.*, 2019, **19**, 3396–3408.
76 E. P. Warekois, M. C. Lavine, A. N. Mariano and H. C. Gatos, *J. Appl. Phys.*, 1962, **33**, 690–696.
77 E. M. Jubeer, M. A. Manthrammel, P. A. Subha, M. Shkir, K. P. Biju and S. A. AlFaify, *Sci. Rep.*, 2023, **13**, 16820.
78 B. Xiao, T. Lv, J. Zhao, Q. Rong, H. Zhang, H. Wei, J. He, J. Zhang, Y. Zhang and Y. Peng, *ACS Catal.*, 2021, **11**, 13255–13265.
79 F. Kayaci, S. Vempati, I. Donmez, N. Biyikli and T. Uyar, *Nanoscale*, 2014, **6**, 10224–10234.
80 C. G. Van de Walle, *Phys. B*, 2001, **308**, 899–903.
81 A. Janotti and C. G. Van de Walle, *Phys. Rev. B: Condens. Matter Mater. Phys.*, 2007, **76**, 165202.
82 H. Oguri, Y. Li and A. Nakamura, *J. Am. Ceram. Soc.*, 2025, **108**, e20338.
83 S. P. Genlik, R. C. Myers and M. Ghazisaeidi, *Phys. Rev. Mater.*, 2025, **9**, 054604.
84 A. Nakamura, X. Fang, A. Matsubara, E. Tochigi, Y. Oshima, T. Saito, T. Yokoi, Y. Ikuhara and K. Matsunaga, *Nano Lett.*, 2021, **21**, 1962–1967.
85 H. Wang, S. I. Morozov, W. A. Goddard Iii and Q. An, *Phys. Rev. B*, 2019, **99**, 161202.
86 K. Matsunaga, S. Hoshino, M. Ukita, Y. Oshima, T. Yokoi and A. Nakamura, *Acta Mater.*, 2020, **195**, 645–653.
87 Y. Shen, M. Li, K. Luo, Y. Zou and Q. An, *J. Am. Ceram. Soc.*, 2025, **108**, e20249.
88 K. Luo, R. Zhou and Q. An, *ACS Mater. Lett.*, 2024, **7**, 46–51.
89 Y. Li, X. Fang, E. Tochigi, Y. Oshima, S. Hoshino, T. Tanaka, H. Oguri, S. Ogata, Y. Ikuhara, K. Matsunaga and A. Nakamura, *J. Mater. Sci. Technol.*, 2023, **156**, 206–216.
90 E. Y. Gutmanas, N. Travitzky and P. Haasen, *Phys. Status Solidi A*, 1979, **51**, 435–444.
91 D. K. Schroder, *IEEE Trans. Electron Dev.*, 2002, **44**, 160–170.
92 R. Häcker and A. Hangleiter, *J. Appl. Phys.*, 1994, **75**, 7570–7572.
93 S. Gupta, M. Y. Frankel, J. A. Valdmanis, J. F. Whitaker, G. A. Mourou, F. W. Smith and A. R. Calawa, *Appl. Phys. Lett.*, 1991, **59**, 3276–3278.
94 H. P. Li, C. H. Kam, Y. L. Lam and W. Ji, *Opt. Commun.*, 2001, **190**, 351–356.
95 B. Hamilton, A. R. Peaker and D. R. Wight, *J. Appl. Phys.*, 1979, **50**, 6373–6385.
96 S. Z. Karazhanov, P. Ravindran, A. Kjekshus, H. Fjellvåg, U. Grossner and B. G. Svensson, *J. Appl. Phys.*, 2006, **100**, 043709.
97 M. V. Fischetti and S. E. Laux, *J. Appl. Phys.*, 2001, **89**, 1205–1231.
98 H. E. Ruda and B. Lai, *J. Appl. Phys.*, 1990, **68**, 1714–1719.
99 M. A. Gilleo, P. T. Bailey and D. E. Hill, *Phys. Rev.*, 1968, **174**, 898.

100 A. Cavallini, P. Gondi and A. Castaldini, *Phys. Status Solidi A*, 1975, **32**, K55–K58.
101 G. C. Kuczynski, K. R. Iyer and C. W. Allen, *J. Appl. Phys.*, 1972, **43**, 1337–1341.
102 K. H. Küsters and H. Alexander, *Phys. B*, 1983, **116**, 594–599.
103 B. Sieber, J. L. Farvacque, J. Wang and J. W. Steeds, *Mater. Sci. Eng. B*, 1993, **20**, 29–32.
104 S. Koubaïti, C. Levade, G. Vanderschaeve and J. J. Couderc, *Philos. Mag. A*, 2000, **80**, 83–104.
105 S. Hoshino, S. Oi, Y. Ogura, T. Yokoi, Y. Li, A. Nakamura and K. Matsunaga, *Phys. Rev. Mater.*, 2024, **8**, 093605.
106 L. Hu, J. Yang, J. Wang, P. Cheng, L. O. Chua and F. Zhuge, *Adv. Funct. Mater.*, 2021, **31**, 2005582.
107 J. Yang, L. Hu, L. Shen, J. Wang, P. Cheng, H. Lu, F. Zhuge and Z. Ye, *Fundam. Res.*, 2024, **4**, 158–166.